AD NUMBER
AD357548
CLASSIFICATION CHANGES
TO: **UNCLASSIFIED**
FROM: **CONFIDENTIAL**
LIMITATION CHANGES
TO: **Approved for public release; distribution is unlimited. Document partially illegible.**
FROM: **Distribution: Further dissemination only as directed by Director, Defense Atomic Agency, Washington, DC 20301, 25 FEB 1965, or higher DoD authority. Document partially illegible.**
AUTHORITY
DNA ltr 6 Dec 1985 ; DNA ltr 6 Dec 1985

Operation

SUN BEAM

SHOT JOHNIE BOY

PROJECT OFFICERS REPORT—PROJECT 1.5

MASS DISTRIBUTION MEASUREMENTS (U)

A. D. Rooke, Jr., Project Officer

G. B. Clark
J. N. Strange

U.S. Army Engineer Waterways
Experiment Station
Vicksburg, Mississippi

Issuance Date: February 25, 1965

Inquiries relative to this report may be made to

Director, Defense Atomic Support Agency
Washington, D. C. 20301

When no longer required, this document may be destroyed in accordance with applicable security regulations.

DO NOT RETURN THIS DOCUMENT

USAEC Division of Technical Information Extension, Oak Ridge, Tennessee

POR – 2282
(WT - 2282)

OPERATION SUN BEAM

SHOT JOHNIE BOY

PROJECT OFFICERS REPORT—PROJECT 1.5

MASS DISTRIBUTION MEASUREMENTS (U)

A.D. Rooke, Jr., Project Officer
G.B. Clark
J.N. Strange

U.S. Army Engineer Waterways
Experiment Station
Vicksburg, Mississippi

ABSTRACT

An array of 186 sheet-metal collector pads was placed in a concentric circular pattern about ground zero (GZ) of a near-surface nuclear explosion. The detonation, with a yield of approximately 0.5 kt (4.53×10^5 kg), occurred at a depth of 58 cm in desert alluvium. After the shot, when residual radioactivity permitted, samples of ejecta and dust (throwout) deposited on these collectors were obtained, weighed, and analyzed for particle size. One hundred samples were thus recovered at distances ranging from 50 to 600 meters from GZ. In ballistic trajectories, large particles were found to have traveled the greatest distances; deposition of very fine particles on the outermost rings is postulated to have occurred at least partially as a result of the base surge. Mass (weight) distribution of throwout per unit area is tabulated and shown graphically as a function of radial distance from GZ, and comparisons with similar experiments are made.

Effects of yield, depth of charge burial, and other variables upon the ejecta equation are examined, as are means of expressing the equation itself. Methods of

predicting both ejecta areal density and thickness are presented and discussed, as are relations between certain mechanics of crater formation, crater volume, and ejecta volume.

CONTENTS

FIGURES

NOTATION

b	a coefficient for the dimensionless expression of the ejecta equation
c	a coefficient for the ejecta equation written for dimensionless distance from GZ, kg/m^2
d	particle diameter
d_a	apparent crater depth, meters
d_o	effective diameter of an ejecta particle
d_t	depth of true crater, meters
dv, dt, etc.	first derivatives of the quantities shown
D , $\vec{D}$	drag force
f	function
$\vec{F}_g$	gravitational force
g	acceleration due to gravity, m/sec^2
h	height above ground surface, meters
$\vec{i}$	unit vector in x-direction
$\vec{j}$	unit vector in y-direction
k	a coefficient in the hyperbolic expression of the ejecta equation, $\delta = k R^m$
k_1	a constant
$\vec{k}$	unit vector in z-direction

m	an exponent in the ejecta equation denoting decay of ejecta areal density with increasing radial distance from GZ
M	mass of ejecta particle
M'	effective mass of ejecta particle
M_a	mass of the apparent crater volume, kg
M_e	mass of ejecta, kg
n	an exponent
r	common ratio of a geometric progression
r_a	apparent crater radius, meters
r_t	true crater radius, meters
$\bar{r}$	radius vector describing the position of a particle of ejecta; i.e. the magnitude and direction of its slant range from the origin
R	radial distance (range) from GZ, meters
R_o	radial distance from GZ to the crater lip crest, meters
R_p	the horizontal distance traveled by an ejecta particle from its original position in the crater, meters
t	time after detonation, sec
t_e	thickness of ejecta deposition, meters

$\vec{u}$	the velocity of an ejecta particle with respect to the ground
v	velocity at any given time
v_i	terminal velocity for a particle in intermediate flow conditions
v_o	initial velocity
v_s	terminal velocity for a particle in streamline flow conditions
v_t	terminal velocity
v_{tu}	terminal velocity of a particle in turbulent flow conditions
v_{xi}	initial horizontal velocity
$v_{x\ ,\ y}$	velocity at any time parallel to the x- or y-axis
$\vec{v}$	the velocity of an ejecta particle with respect to the air (or medium) mass
V_a	apparent crater volume, m^3
V_{cf}	that part of the volume of a crater caused by compression and plastic flow, m^3
V_e	volume of ejecta, m^3
V_i	volume of ejecta at some value of R/r_a, m^3
V_t	true crater volume, m^3

V_w , $\vec{V}_w$	wind velocity
W	charge weight or yield expressed as equivalent weight of TNT, kt or kg
x , y , z	axes of a three-dimensional coordinate system
Z	scaled position of charge with reference to the earth-air interface
Z'	scaled <u>depth</u> of burst, $ft/kt^{1/3.4}$ or $m/kg^{1/3}$
α	the specific value of ϕ which describes the direction of a constant horizontal wind, degrees
γ	specific weight (density) of ejecta, kg/m^2
δ	ejecta areal density; mass (weight) distribution, kg/m^2
ζ	a coefficient
θ	angle of elevation of ejected particle, measured from the vertical, degrees
θ_o	angle of elevation of ejected particle at the instant of ejection, degrees
θ_1	angle between an ejecta particle velocity vector and the horizontal
θ_{1_o}	the angle between a particle velocity vector and the horizontal at the instant of ejection

K	a constant associated with the dimensional expression for drag force on a particle following a trajectory in a fluid
K_i	the constant K as applied to intermediate flow conditions
K_s	the constant K as applied to streamline flow conditions
K_t	the constant K as applied to turbulent flow conditions
λ	mean free path of air molecules
μ	viscosity of a given medium
π	a constant, ≈ 3.1416
ρ	particle density
ρ_o	density of the air
σ	strength properties of the cratered medium
ϕ	angle between the z-axis and the xz plane, degrees
∞	infinity

One dot $(\cdot)$ denotes the derivative with respect to time $\left(\frac{d}{dt}\right)$. Two dots $(\cdot\cdot)$ denote the second derivative with respect to time.

CHAPTER 1

INTRODUCTION

1.1 OBJECTIVE

The objective of Project 1.5 was to determine the distribution of crater ejecta (throwout) resulting from the detonation of a low-yield, near-surface nuclear device in desert alluvium, including the distribution by weight (or mass) and grain size.

1.2 BACKGROUND

The mass movement of earth materials by surface and near-surface nuclear detonations is of military significance primarily because of its effects upon nearby military installations, especially those "hardened" to survive near-misses of nuclear warheads. Damage caused by ejecta striking or covering antennas, missile site components, entrances to protective structures, etc., presents a definite hazard. The behavior of ejected material is also of interest in peacetime projects involving nuclear energy, such as the excavation of canals, harbors, etc.

The history of ejecta experiments shows a wide variety of environmental conditions. Because of the variation in

media, data which are ultimately to be employed to support scientific hypotheses will probably require treatment by statistical methods, establishing probabilities, randomness or variation, interdependence of variables, mean values, standard deviations, and similar statistical parameters. There is also a need for a more quantitative definition of the parameters governing ejecta deposition, as well as their association with scaled depth of burst, crater radius and depth, etc. The solution of these problems will require a large amount of data. The Johnie Boy shot provided a means of augmenting the information available from the studies discussed below and was of particular significance because of its near-surface geometry.

Prior to Johnie Boy, 43 cratering shots had been made which furnished usable crater-ejecta data. Several studies have been made (References 1 through 10) of the areal deposition and particle size distribution of throwout from craters produced by explosive charges ranging in size from a few hundred pounds to 0.5 kt of high explosive (HE) and from 0.42 to 100 kt of nuclear explosive (NE). These studies have in some cases been included as primary projects and in other cases as secondary investigations. Charge positions

have varied from that of a contact burst (resting upon ground surface) to a scaled depth of 0.68 $m/kg^{1/3}$ (216 $ft/kt^{1/3}$) in several types of soil and rock. Forty shots have been HE and three NE. Synopses of these investigations are provided in the following paragraphs.

1.2.1 Engineering Research Associates, Inc. (ERA). ERA dust (ejecta) studies, conducted in Utah, included media of sandstone, limestone, dry sand, dry clay, and wet clay, and were performed with trinitrotoluene (TNT) charges varying in size from 1.45×10^2 to 1.45×10^5 kg (320 to 320,000 pounds) placed at scaled depths of 0.14 to 0.40 $m/kg^{1/3}$ (44 to 127 $ft/kt^{1/3}$). In the sand and clay studies, samples were obtained at distances from ground zero (GZ) of 125 to 500 feet on smaller shots and to distances of approximately 3,100 feet on the larger shots. In the sandstone tests, the sampling range was 50 to 1,000 feet for the small shots and 750 to 5,000 feet for the largest. The single limestone test utilized sampling gages 50 to 250 feet from GZ. Results of these studies are summarized in Reference 1, and additional tabulation and plotting of the data are included in Reference 10.

1.2.2 Suffield Experimental Station (SES). Two contact shots, one of 5 tons and the other of 100 tons of TNT, were fired on the Watching Hill site at the Suffield Experimental Station in Ralston, Alberta, Canada, and throw-out studies were made (References 3 and 4). The surface deposits at this site consist of silt and clay, underlain by soft strata of clay, shale, sandstone, and gravel to a depth of 300 feet.

1.2.3 Nevada Test Site (NTS) Studies--HE Shots. Eight HE cratering-ejecta experiments have been conducted at the U. S. Atomic Energy Commission's Nevada Test Site: Scooter, Stagecoach I and II, White Tribe, Jangle HE-2, and Buckboard 11, 12, and 13. Except for the Buckboard shots, which were in basalt, and White Tribe, which was in caliche, the detonations were conducted in desert alluvium. All were buried shots except White Tribe, which dealt only with contact bursts. Jangle HE-2 was, however, quite near the surface. References 2, 5, 6, 8, and 9 report these events.

1.2.4 NTS Studies--NE Shots. In addition to Johnie Boy, three NE cratering-ejecta experiments have been conducted to date at NTS: Teapot Ess, Danny Boy, and Sedan (References 2, 7, and 10). These three shots involved deeply buried charges and therefore are not

directly comparable to Johnie Boy.

1.2.5 Summary of Ejecta Data. Appendix A summarizes in tabular form all usable cratering-ejecta experiments known to the authors; the tabulation includes also the results obtained from Johnie Boy. Figures 1.1 and 1.2 are selected, normalized ejecta curves from Reference 10.

1.3 THEORY

1.3.1 General. As shown in Reference 10, there is a definite qualitative relation between ejecta distribution and other cratering parameters, such as scaled depth of burst, crater radius, depth, volume, etc. Thus, ejecta parameters are affected by many of the same factors that affect true and apparent crater formation, as well as by weather (wind and, to a lesser degree, precipitation). That is, apparent crater volume is dependent upon the size of the true crater and upon the volume of the fallback material. The apparent crater results from (1) ejection of material from the crater, (2) flowage of material into the upthrust region which lies beneath the crater lip, and (3) compression of the in situ material that lies just beyond the boundary of the true crater.

Charge parameters include size, energy density, shape, velocity of detonation, the pressure-time history of the developed gas bubble, thermal properties, efficiency, depth of burial, and effective or scaled depth. Medium parameters include density, strengths, homogeneity, compressibility, stress wave attenuation properties, viscosity, and directly related gravity effects.

Particle size distribution of the ejecta and its relation to air drag and wind effects are important elements in determining the distance particles of a given size will travel from the crater. For large particles (missiles), ballistic trajectories are determined by the initial velocities imparted to the particles, the angles of elevation of the trajectories, and the drag resistance of the atmosphere. For small particles, the settling (terminal) velocities in relation to wind become important. Thus the velocity field generated by the explosion in the cratered material and the degree of comminution largely determine the particle trajectories and the distances the particles will travel from their initial positions within the crater.

1.3.2 Cratering by Shallow Bursts. The interrelation between cratering mechanisms varies with scaled depth of

burst and the characteristics of the cratered medium. For shallow bursts in sand and fine-grained soil, the mechanism is dominantly that of viscous flow, and it is assumed to be similar for tuff and alluvium. Reference 11 reports a computer program developed for a theoretical model of a 2-Mt surface burst, assuming that the input required (1) the history of the nuclear explosion, (2) an equation of state for the earth medium, and (3) an estimation of the energy partitioning. A hydrodynamic model was employed in the early stages, and gravity was not a consideration in the crater formation. The usual hydrodynamic equations for shock phenomena were employed to describe the conservation of mass, momentum, and energy, with a pressure function of two variables, density and specific internal energy. Effects of heat conduction and viscosity were neglected, although it has been postulated (Reference 12) that viscous effects and a consequent 1/2-power scaling law may dominate the formation of craters that are produced by very large surface bursts. The shock energy was governed by Hugoniot conditions. Results obtained on the two-dimensional model thus established were found to be in reasonable agreement with experimental observations.

Although the model was developed for a 2-Mt burst in tuff, the results should apply in principle to the Johnie Boy experiment. Theoretically, the pressures and temperatures of a small burst should be the same as those of a large burst, analagous to the process of detonation of chemical explosives (HE), where the peak temperature and pressure are independent of the charge size, provided optimum detonation velocity is achieved. It would also be expected that the vectors in the velocity field would be geometrically similar for identical scaled depths of burst of the same explosive, with adjustments made for the actual and gravity-induced differences in the properties of the media.

As a result of the very high pressures generated by a nuclear explosion, alluvium not only flows but is considerably compressed. It is estimated in Reference 2 that compression of the surrounding material accounted for 41 percent of the apparent volume of the Sedan crater. However, Reference 13 indicates that the size of an explosion crater is not materially affected by volumetric changes of the soil within which the crater is formed. It appears logical to assume that the soil is temporarily compressed, but recovers most of its original volume, and that the apparent crater

volume comprises principally contributions of ejecta volume and plastic flowage of the soil.

The intense pressure of the detonation undoubtedly causes both fusion and pulverization of surrounding soil and rock. Small particles of ejecta are more severely affected by air resistance, and settling velocities relative to wind velocity determine the distances to which small particles will be carried. While no exact quantitative relations can be derived theoretically concerning ejecta distribution, velocity fields, and wind effects, a discussion of the basic principles involved is given in Appendix B in order to offer a partial, qualitative explanation and to indicate the areas of need for more fundamental research.

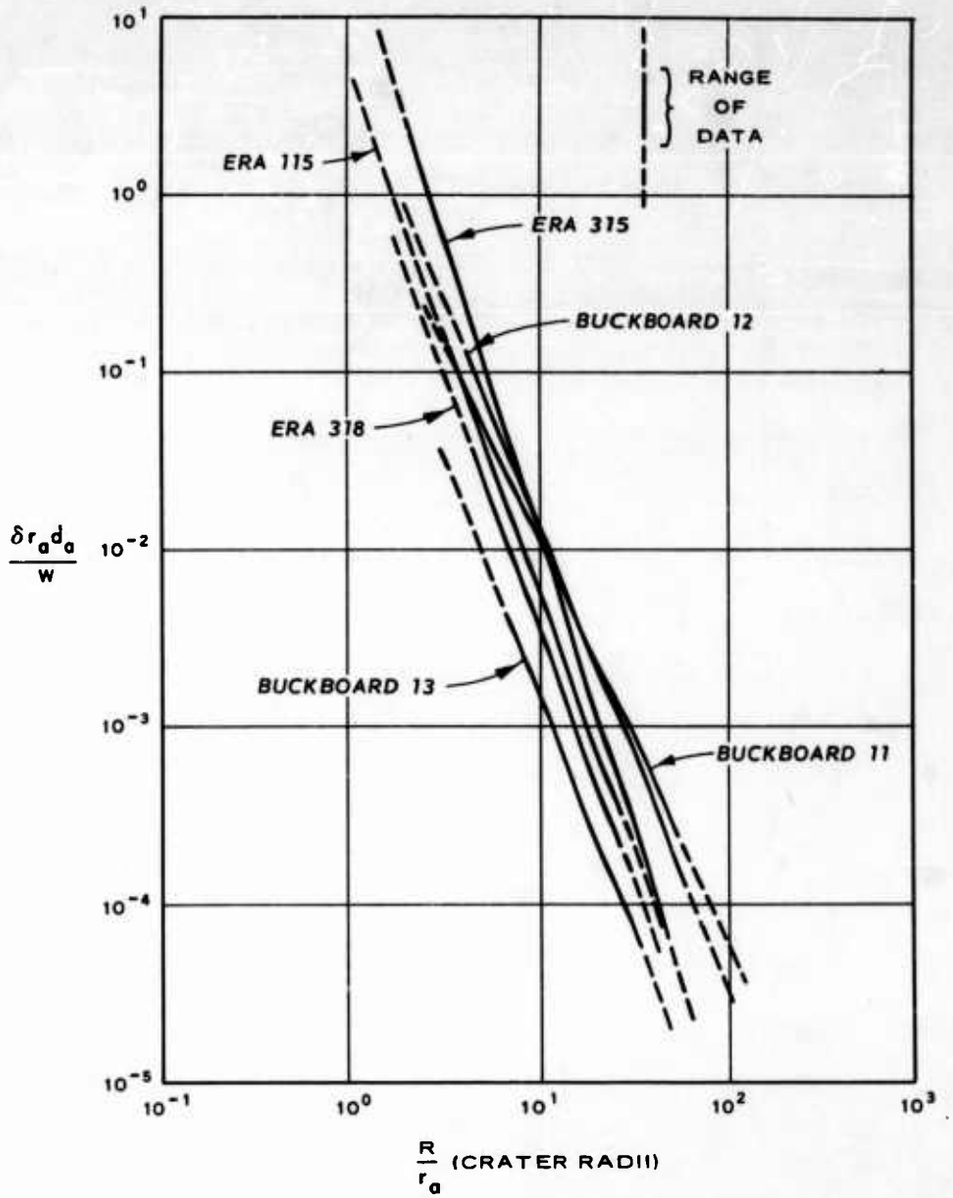

Figure 1.1 Comparison of ERA and Buckboard ejecta curves (Reference 10).

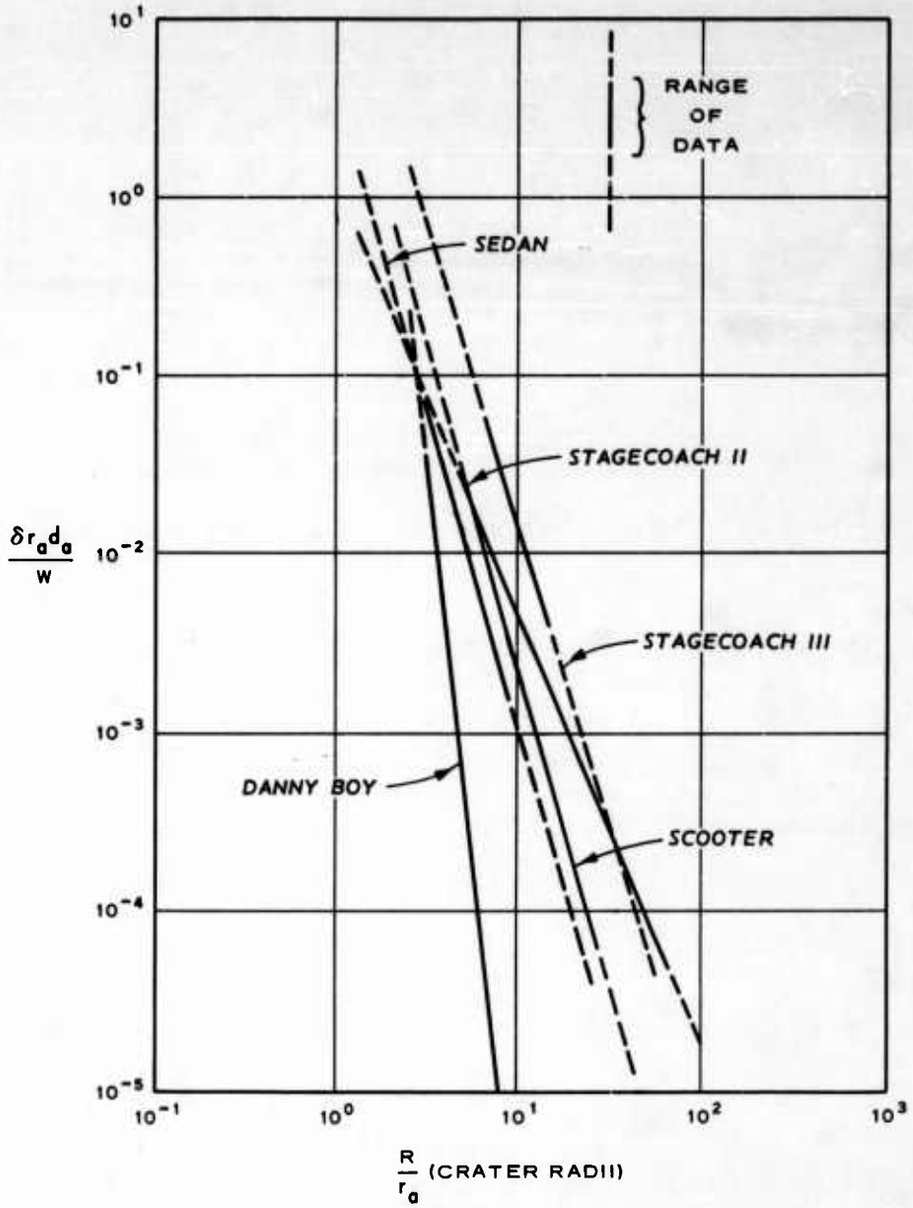

Figure 1.2 Comparison of Stagecoach, Scooter, Sedan, and Danny Boy ejecta curves (Reference 10).

CHAPTER 2

PROCEDURE

2.1 SITE LOCATION

The Johnie Boy event was conducted in area 18 of the NTS (see Figure 2.1).

2.2 ENVIRONMENTAL CONDITIONS

The test area was a relatively flat portion of an alluvial fan. The soil was gravelly sand, containing numerous cobbles and exhibiting some cementation; there was little variation in its composition to a depth of at least 80 feet, the deepest boring made by personnel of the Soils Division, U. S. Army Engineer Waterways Experiment Station (WES), during the soils survey. Soil density, measured near GZ, was approximately 1,870 kg/m^3 (117 lb/ft^3). The rather sparse vegetation in the area consisted mostly of sagebrush.

The measured properties of the soil (Reference 14) at the Johnie Boy site include stratification, soil type, water content, mineral content, density, and particle size distribution. Samples taken in the vicinity of GZ showed gravelly sand with cobbles to a depth of 30 feet, with sand and occasional cobbles to the full depth of the hole. Depth of the

stratum with largest percentage of cobbles varied, being generally greatest near GZ. Because of difficulties caused by cobbles during the drilling of the upper 20 feet of the soil, samples from this region are not considered truly representative.

Mineralogical analysis showed that the larger sieve sizes were composed of dense, light gray to pink volcanic rocks, vesicular porphyries, and glassy particles. Almost all of the particles were coated with a calcareous covering. In general the samples consisted principally of rocks ranging from soda dacite to rhyolite, with textures ranging from porphyries to tuffs and highly glassy rocks with flow structures shown in elongated pebbles.

The particle size curves in Reference 14 show much more fine material below 30 feet, with an increase of plus No. 10 material above this level. For the near-surface detonation of the Johnie Boy device, it would be expected that most of the ejecta would come from above the 30-foot depth.

2.3 EXPERIMENTAL ARRAY

2.3.1 Geometry. A circular pattern of throwout collectors (see Figure 2.2) was chosen due to (1) the somewhat

unpredictable wind spectrum, and (2) the random circumferential variation in throwout deposition known to have occurred in previous experiments. The greatest radial distance (600 meters) was chosen to represent 30 predicted crater radii, the maximum distance at which recovery of identifiable ejecta samples was anticipated. The minimum distance (50 meters) was selected to fall slightly outside the predicted crater lip. The choice of seven circular rings of collector pads was an arbitrary one, based largely upon limitations of time and funds. With the foregoing conditions fixed, it was assumed that throwout deposition would decrease with increasing radial distance from GZ as a geometric progression of common ratio, r . Therefore, $r^6 = \frac{600}{50}$, and $r \approx 1.5$, the multiplier used to determine the radial distances of the rings between 50 and 600 meters. The number of collectors on each ring was approximately proportional to the circumference of the ring, beginning with a minimum of 12 on the three inner rings. A total of 186 collectors was included in the array.

2.3.2 Placement and Numbering of Collectors. Each collector consisted of a 2.50-by-3.00-foot (0.70 m^2) sheet-metal pad. Survey for the collector layout was provided by

Holmes and Narver, on-site architect-engineers, who marked all collector stations by means of coded stakes. Where necessary, a small area was cleared at each station, and collectors were roughly leveled and oriented. In some cases, as when stations fell on or near roads, the collector position was moved to one side far enough to prevent its being disturbed. Spikes driven through predrilled holes in the metal pads served to secure collectors in place. In addition, collectors on the three innermost rings, which were subjected to the greatest blast and shock, were set in concrete. The rings were lettered in alphabetical order, beginning with A as the closest to GZ, and collectors on each ring were numbered in clockwise fashion, number 1 being the first station east of true north. Figure 2.3 is an aerial view of the Johnie Boy site during preshot construction, in which a portion of the Project 1.5 layout is visible. To guard against preshot accumulation of debris, regular inspections of the collector rings were made until just prior to shot time.

2.4 TEST CONDITIONS

The Johnie Boy shot was detonated at 0945 hours,

11 July 1962. The weather was clear and warm, surface temperature and relative humidity being recorded as 24.3 degrees C and 12 percent, respectively. Surface winds were from the south (195 degrees) at about 6 knots (7 mph). [redacted] shot yield was [redacted] shown in Figure 2.4.

2.5 RECOVERY OF THROWOUT SAMPLES

It was important that the particulate deposition on the collectors be recovered as soon as possible, in order to minimize the effects of weather on the fine materials. Initially, residual radiation made it necessary that examination of the collectors be limited to the outer rings and to the southern portion of the array. Recovery began on D + 1 (12 July) and continued intermittently (as radiation levels permitted) until 26 July, at which time 135 collectors had been examined and 73 samples recovered. The remainder of the recovery work was accomplished on 11 October. Of the 186 collectors, 100 samples were obtained, 21 collectors were destroyed or buried by debris so as to make recovery impracticable, and 3 collectors were found to have been disturbed so as to render any samples on them useless. The

remainder (62) contained no identifiable deposition. Several of the close-in pads had been dislodged by the force of the blast, but the concrete bases were found in place, and samples were taken from these. The initial effort was toward recovery of the maximum number of specimens in the shortest time possible. Therefore, samples were sealed in metal containers, which were marked and left in place. They were later removed to a shelter about 4,000 feet from GZ, where initial weighing was accomplished and data sheets were prepared. The samples were then resealed and stored for later sieve analysis. Figures 2.5 and 2.6 show the recovery and weighing operations. The extent of sample recovery is graphically illustrated in Figure 2.7.

2.6 SIEVE ANALYSES

WES Soils Division personnel performed sieve analyses on 99 throwout samples (one was lost in handling) in February 1963. For this purpose, the sealed samples were transported to CP-2 at NTS, the location of Reynolds Electrical and Engineering Company's Rad-Safe office. Here they were stored and processed in a shelter and trailer set aside for that purpose and under conditions designed to facilitate

radioactivity control and safety measures. U. S. standard sieves and a mechanical shaker were used. A second, more accurate weight was also obtained on each specimen. Small samples were analyzed in their entirety, while standard quartering procedures were employed to reduce large samples to a more convenient size.

2.7 INVESTIGATION OF CRATER LIP

In June 1963, in conjunction with a study of crater measurements, excavations were made in the region of the crater lip to define the interface between the upthrust original ground surface and the ejecta overburden. Figure 2.8 shows the area of this investigation, which was taken to a distance of 46 meters (150 feet) from GZ. At the greater distances, small pits were dug, and the ejecta thicknesses were measured. Where the crater lip was well defined, trenches were dug extending north, east, and south of the crater (to the west, excavation had already occurred on another project), and the original ground surface was mapped by means of conventional survey. The profile of the crater lip, including the ejecta overburden, was also surveyed. Apparent sliding and folding of bedding planes near the crater edge made identification of the ground surface-ejecta interface uncertain in some places. Observations made by WES Geology Branch personnel are included as Appendix C.

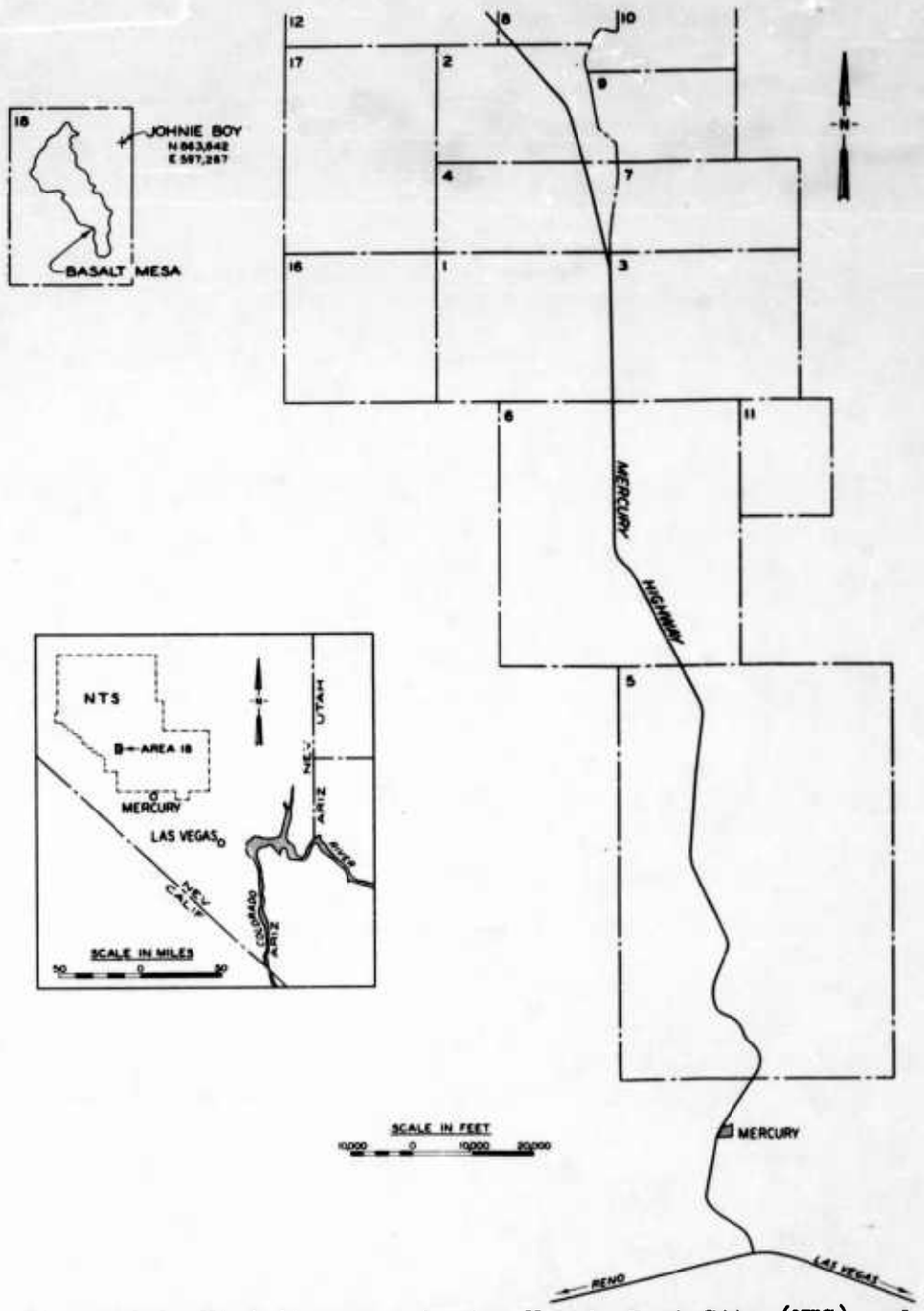

Figure 2.1 Vicinity map, showing Nevada Test Site (NTS) and the location of the Johnie Boy event in Nevada state coordinates. Numerals are NTS area numbers.

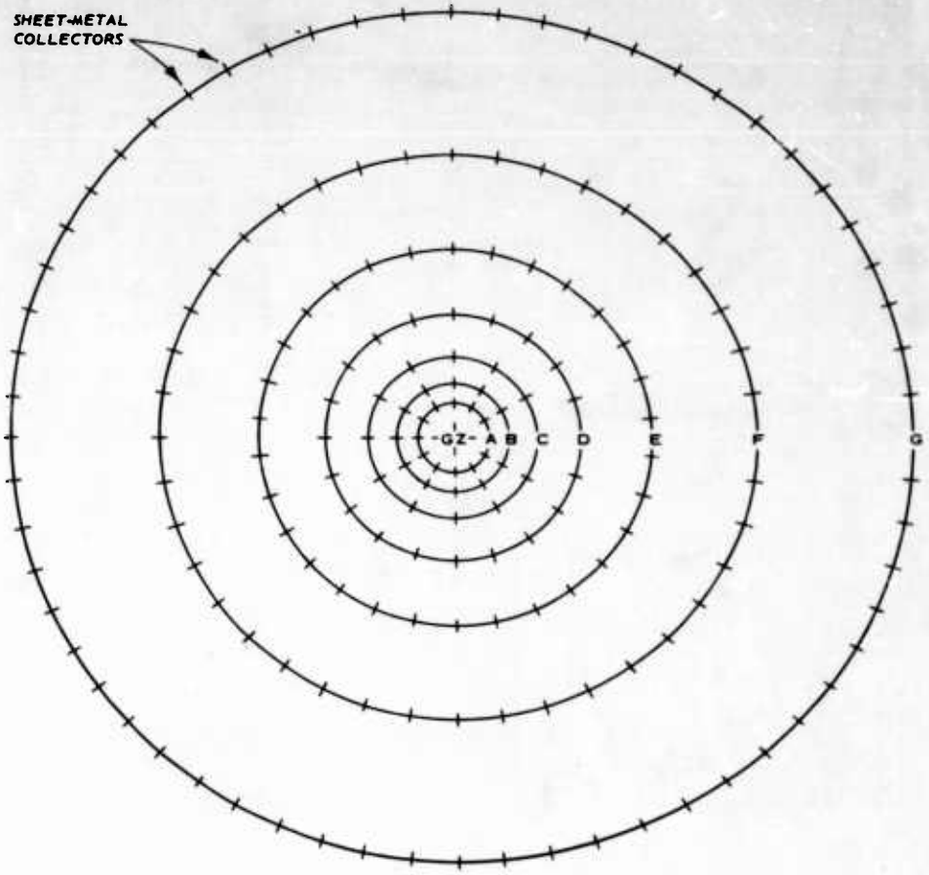

RING	DISTANCE FROM GZ METERS	ANGULAR INTERVAL DEGREES
A	50	30
B	75	30
C	115	30
D	175	18
E	265	12
F	400	9
G	600	6

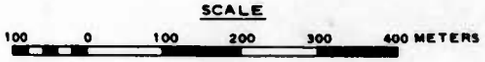

Figure 2.2 Layout of experimental array.

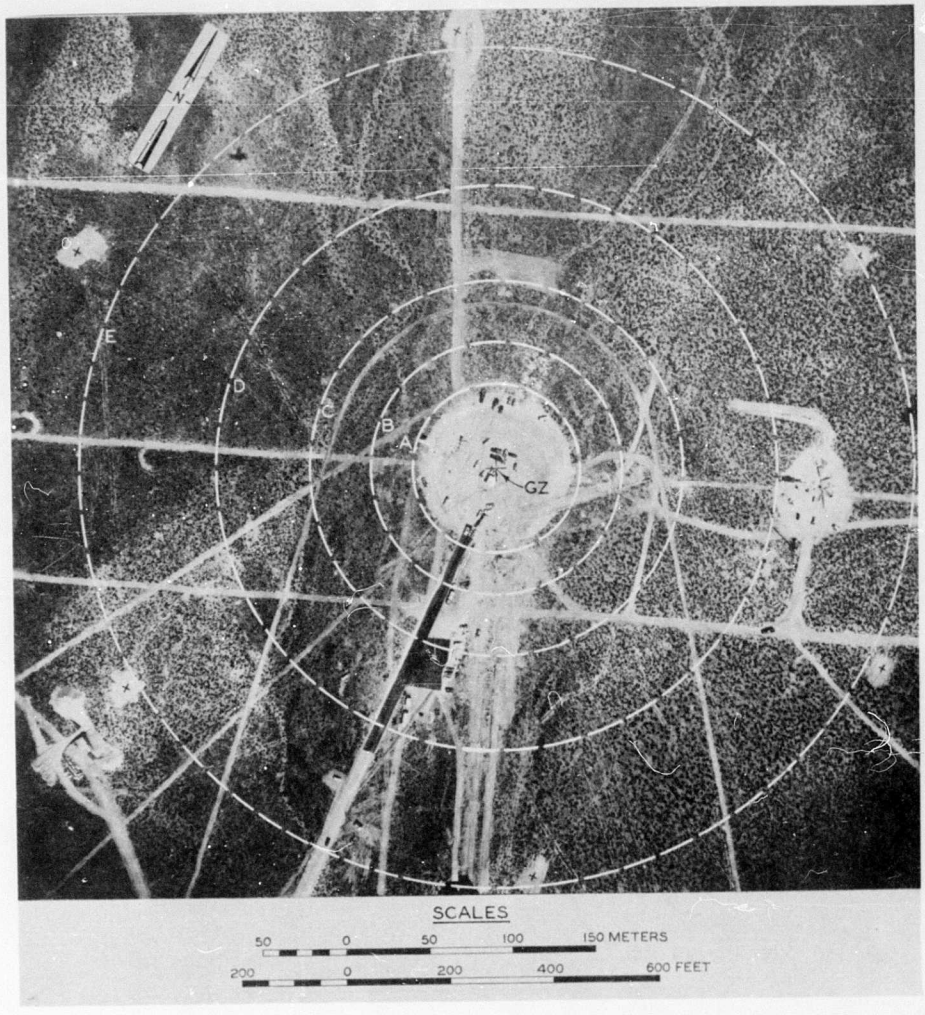

Figure 2.3 Aerial view of Johnie Boy site, showing part of Project 1.5 layout. Activity is preshot survey, construction, etc. Note concrete crosses used for ground reference stations. Apparent asymmetry in layout is caused by distortion in photograph.

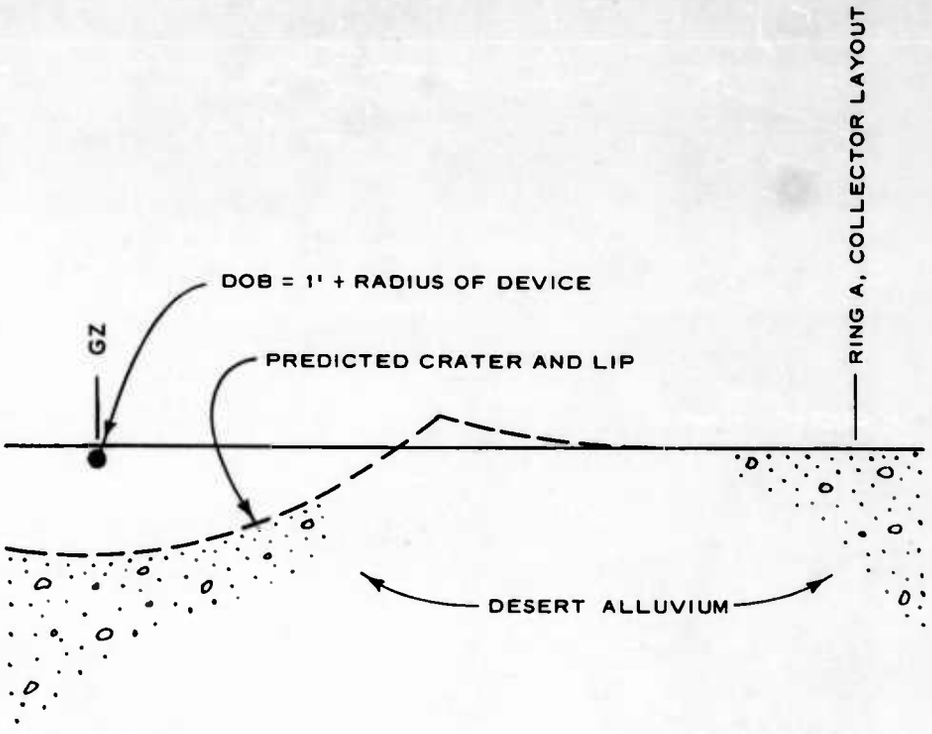

NOTE: YIELD ≈ 0.5 KT.

Figure 2.4 Shot geometry, Johnie Boy.

Figure 2.5 Typical sample recovery.

Figure 2.6 Initial weighing and recording of samples. The Howe scale had a 300-pound capacity in 1/4-pound graduations; the Soiltest scale (in use) had a 35-pound capacity in 0.01-pound graduations.

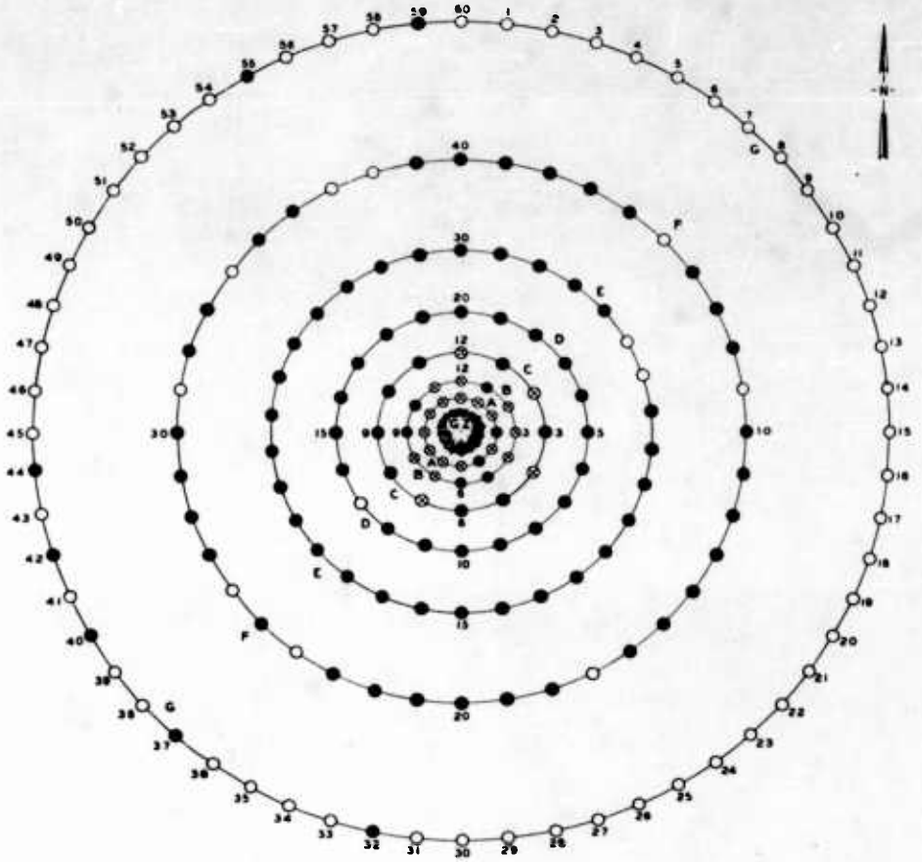

RING	DISTANCE FROM GZ METERS	DISTANCE FROM GZ FEET	NUMBER STATIONS	ANGULAR INTERVAL DEGREES
A	50	1640	12	30
B	75	2460	12	30
C	115	3772	12	30
D	175	5740	20	18
E	265	8692	30	12
F	400	13120	40	9
G	600	19680	60	6

LEGEND

- ● COLLECTOR STATION; SAMPLE RECOVERED
- ○ COLLECTOR STATION; NO SAMPLE RECOVERED
- ⊗ COLLECTOR DESTROYED OR LOST UNDER LIP

SCALES

-100 0 100 200 300 400
METERS
-200 0 200 600 900 1200
FEET

Figure 2.7 Ejecta sample recovery.

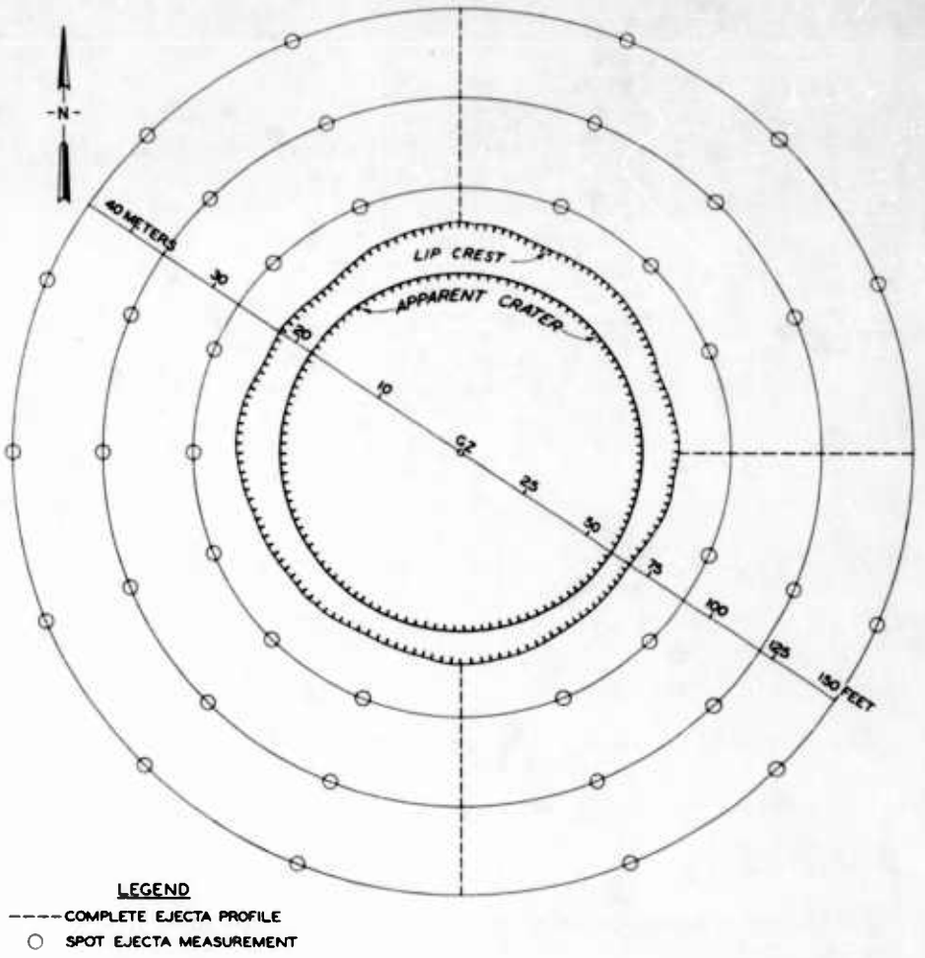

Figure 2.8 Close-in investigation of ejecta deposition.

CHAPTER 3

RESULTS

3.1 MASS DISTRIBUTION

Figure 3.1 is an aerial stereopair of the Johnie Boy crater, showing the lip and the general pattern of ejecta distribution. Weights of recovered samples are given in Table 3.1. Recovery of ejecta samples from the A ring was poor due to the effects of the blast and to the ejecta thickness, which made it difficult to locate the collector pads. The recovery for rings B through G was satisfactory; however, some of the collectors on F and most of those on G had no readily discernible ejecta deposited on them. The sample weight data are also presented graphically on an ejecta distribution map (Figure 3.2). Although at shot time there was a 7-mph wind from 195 degrees true azimuth, it had no apparent effect upon ejecta distribution.

The thickness of ejecta deposition near the crater lip is shown, together with the upthrust of the ground surface, in Figure 3.3. Tables 3.2 and 3.3 give ejecta thicknesses in the region of the crater lip. These data were obtained on three radials only, and they provide a general

representation of ejecta profiles, which actually exhibited a considerable circumferential variation. For detailed profiles of the lip crest, see Appendix C. Preshot and postshot contour maps were employed to calculate the total vertical change in surface elevation near the crater (see Figure 3.4). The contours in Figure 3.4 reveal the amount of upthrust and throwout; they were obtained by referring all elevations to a horizontal plane through the (preshot) GZ.

3.2 PARTICLE SIZE DISTRIBUTION

Each sample was screened through U. S. standard screen sizes 1-1/2-inch, 3/4-inch, No. 10, and No. 200, or with Nos. 8 and 16 in place of No. 10 (see Table 3.4). For purposes of analysis and graphical comparison, the screen fractions obtained with Nos. 8 and 16 were converted to an approximate distribution corresponding to that for No. 10 only by placing one-quarter of the No. 16 fraction with the No. 8 fraction and the remaining three-quarters with plus No. 200. The adjusted No. 8 fraction was then assumed to define the No. 10 fraction.

The cumulative distribution for each ring was

calculated using the total weight of each screen fraction for all samples in the ring. For the F and G rings, however, samples F-1 and G-32 were omitted from the calculations because their weights were very large compared with the other samples in those rings, and their inclusion would have biased the values of the cumulative distributions. Their omission is permissible because the total cumulative distribution gives weight in proportion to the weights of the individual screen fractions, and any statistical treatment to determine significant samples requires that the samples obtained be representative of the population from which they are drawn. As each ring was selected to represent a stratum which was presumably homogeneous in character, those samples which do not fall into the pattern of homogeneity may be rejected. Although there are mathematical tests to determine the acceptability of samples, the general character of the data here does not seem to justify the application of detailed, rigorous mathematical criteria.

The cumulative particle size distributions of the composite ring samples and those for the in situ alluvium (from Reference 14) are shown in Figure 3.5.

3.3 EJECTA PHOTOGRAPHY

Six photographs of the fireball and early trajectory history of the Johnie Boy shot, taken for a project conducted by Edgerton, Germeshausen, and Grier, Inc. (EG&G), show the phenomena accompanying the near-surface burst at times ranging from 0.48 to 5.62 sec after detonation (Figure 3.6).

TABLE 3.1 MASS DISTRIBUTION OF EJECTA

Station	Radial Distance from GZ	Field Weight of Specimen	Metric Weight of Specimen	Ejecta Distribution per Unit Area
	meters	lb	kg	kg/m^2
A-3	50	12.80	5.82	8.35
A-5		28.00	12.73	18.26
B-1	75	35.5	16.14	23.16
B-5		2.70	1.23	1.76
B-6		9.50	4.32	6.20
B-9		22.50	10.23	14.68
B-10		12.00	5.45	7.82
C-1	115	7.10	3.23	4.63
C-3		3.30	1.50	2.15
C-5		2.90	1.32	1.89
C-6		1.12	0.50	0.72
C-8		0.55	0.25	0.36
C-9	115	4.10	1.86	2.67
C-10		79.0	35.90	51.51
C-11		4.61	2.09	3.00
D-1	175	4.30	1.95	2.80
D-2		14.90	6.77	9.71
D-3		5.60	2.54	3.65
D-4		3.22	1.46	2.10
D-5		1.99	0.90	1.29
D-6	175	0.40	0.18	0.26
D-7		0.41	0.19	0.27
D-8		0.24	0.11	0.16
D-9		5.23	2.37	3.40
D-10		6.08	2.74	3.93
D-11	175	2.74	1.24	1.78
D-12		0.31	0.14	0.20
D-14		0.25	0.11	0.16
D-15		1.28	0.58	0.83
D-16		0.62	0.28	0.40
D-17	175	9.81	4.45	6.39
D-18		2.68	1.22	1.75
D-19		9.00	4.09	5.87
D-20		8.35	3.80	5.45
E-1	265	3.95	1.80	2.58
E-2		0.17	0.08	0.11
E-3		1.10	0.50	0.72
E-4		1.92	0.87	1.25
E-7		0.78	0.35	0.50
E-8	265	0.12	0.05	0.07
E-9		0.02	0.01	0.01(-)
E-10		0.34	0.15	0.22
E-11		0.05	0.02	0.03
E-12		3.94	1.79	2.57
E-13	265	0.09	0.04	0.06(-)
E-14		0.02	0.01	0.01(+)
E-15		0.06	0.03	0.04(+)
E-16		0.13	0.06	0.09(-)
E-17		0.08	0.04	0.06(-)
E-18	265	0.06	0.03	0.04(-)
E-19		0.22	0.10	0.14
E-20		0.14	0.06	0.09(-)
E-21		0.10	0.05	0.07
E-22		0.07	0.03	0.04(+)
E-23	265	0.21	0.10	0.14
E-24		0.77	0.35	0.50
E-25		0.73	0.33	0.47
E-26		0.18	0.08	0.12
E-27		0.10	0.05	0.07
E-28	265	1.81	0.82	1.18
E-29		0.51	0.23	0.33
E-30		0.48	0.22	0.32
F-1	400	4.10	1.86	2.67
F-2		0.04	0.02	0.03
F-3		0.09	0.04	0.06
F-4		0.01	0.01	0.01(+)
F-6		0.10	0.05	0.07
F-7	400	0.23	0.11	0.16
F-8		0.04	0.02	0.03(-)
F-10		0.07	0.03	0.04(+)
F-11		0.02	0.01	0.01(+)
F-12		0.10	0.05	0.07
F-13	400	0.13	0.06	0.09(-)
F-14		0.09	0.04	0.06
F-15		0.06	0.03	0.04(-)
F-16		0.06	0.03	0.04(+)
F-18		0.05	0.02	0.03
F-19	400	0.02	0.01	0.01(+)
F-20		0.04	0.02	0.03(-)
F-21		0.05	0.02	0.03
F-22		0.04	0.02	0.03
F-23		0.06	0.03	0.04(-)
F-25	400	0.02	0.01	0.01(+)
F-27		0.08	0.04	0.06
F-28		0.13	0.06	0.09(-)
F-29		0.03	0.01	0.01(+)
F-30		0.05	0.02	0.03
F-32	400	0.92	0.42	0.60
F-33		0.07	0.03	0.04(+)
F-35		0.03	0.01	0.01(+)
F-36		0.06	0.03	0.04(+)
F-39		0.04	0.02	0.03
F-40		0.08	0.04	0.05
G-32	600	0.13	0.06	0.09(-)
G-37		0.15	0.07	0.10
G-40		0.01	0.01	0.01(-)
G-42		0.02	0.01	0.01(+)
G-44		0.02	0.01	0.01(+)
G-55		0.02	0.01	0.01(+)
G-59		0.02	0.01	0.01(-)

TABLE 3.2 EJECTA THICKNESSES AT SELECTED STATIONS

True Azimuth	Ejecta Thickness		
	27.43 meters (90 feet) from GZ	36.57 meters (120 feet) from GZ	45.72 meters (150 feet) from GZ
degrees	meters	meters	meters
22.5	0.46	0.06	0.09
45.0	0.21	0.15	0.15
67.5	0.18	0.27	0.12
90.0	0.55	0.55	0.15
112.5	0.30[a]	0.21	0.12
135.0	0.40	0.12[a]	0.09
157.5	0.30	0.40	0.40
180.0	0.79	0.61	0.15
202.5	0.34	0.12	0.06
225.0	0.18	0.18	0.09
247.5	0.21	0.09	0.09
270.0	0.30	0.24	0.18[a]
292.5	0.12	b	0.18
315.0	0.34	0.12	0.15
337.5	0.61	0.24	0.30
360.0	0.49	0.30	0.12

[a] Area disturbed; thickness estimated.
[b] Area disturbed; no measurement taken.

TABLE 3.3 EJECTA THICKNESS THROUGH CRATER LIP

North (0 Degree True Azimuth from GZ)		East (90 Degree True Azimuth from GZ)		South (180 Degree True Azimuth from GZ)	
Distance from GZ	Ejecta Thickness	Distance from GZ	Ejecta Thickness	Distance from GZ	Ejecta Thickness
meters	meters	meters	meters	meters	meters
23.77	1.83	21.95	0.30	22.16	0.30
24.38	1.92	22.86	0.34	22.86	1.04
25.91	1.34	24.38	0.37	24.38	1.49
27.43	0.49	25.91	0.40	27.43	0.79
28.96	0.64	27.43	0.55	30.48	0.34
30.48	0.49	30.48	0.61	36.57	0.61
33.52	0.49	32.00	0.61	45.72	0.15
36.57	0.30	33.52	0.52		
38.10	0.37	36.57	0.55		
39.62	0.15	39.62	0.15		
45.72	0.12	45.72	0.15		

TABLE 3.4 PARTICLE SIZE DISTRIBUTION BY WEIGHT (POUNDS) OF EJECTA SAMPLED

Ring A						Ring B								Ring C							
Screen Size	A-3	A-5	Total	Cumulative	Percent	Screen Size	B-1	B-5	B-6	B-6a*	B-10	Total	Cumulative	Percent	Screen Size	C-1	C-3	C-3a	C-5	C-6	C-6a	C-8	C-9
1-1/2-inch	0.000	1.335	1.335	12.719	100.00	1-1/2-inch	0.063	0.000	0.240	0.240	0.132	0.435	24.248	100.00	1-1/2-inch	0.000	0.005	0.005	0.600	0.100	0.100	0.000	---
3/4-inch	0.095	0.130	0.225	11.384	89.50	3/4-inch	0.250	0.030	0.202	0.202	0.000	0.482	23.813	98.21	3/4-inch	0.085	0.080	0.080	0.101	0.180	0.180	0.028	0.214
No. 4	0.505	1.148	1.653	11.159	87.73	No. 4	1.250	0.298	1.053	1.053	0.615	3.216	23.331	96.22	No. 4	0.670	0.545	0.545	0.534	0.221	0.221	0.198	0.380
No. 8	---	---	---	---	---	No. 8	---	---	0.543	---	---	---	---	---	No. 8	---	0.225	---	---	0.065	---	---	---
No. 10	0.408	1.039	1.447	9.506	74.74	No. 10	0.960	0.228	---	0.688	0.370	2.246	20.115	82.96	No. 10	0.301	---	0.276	0.221	---	0.079	0.050	0.087
No. 16	---	---	---	---	---	No. 16	---	---	0.660	---	---	---	---	---	No. 16	---	0.205	---	---	0.055	---	---	---
No. 200	3.305	4.350	7.655	8.059	66.90	No. 200	5.965	1.770	6.390	6.905	1.950	16.590	17.869	73.69	No. 200	1.250	1.965	2.119	1.231	0.366	0.407	0.210	0.345
Passing No. 200	0.317	0.087	0.404	0.404	3.18	Passing No. 200	0.080	0.377	0.410	0.410	0.412	1.279	1.279	5.27	Passing No. 200	0.202	0.225	0.225	0.182	0.132	0.132	0.047	0.132
Total	4.630	8.089	12.719	---	---	Total	8.568	2.703	9.498	9.498	3.479	24.248	---	---	Total	2.508	3.250	3.250	2.869	1.119	1.119	0.533	1.158

Ring C (Continued)						Ring D																	
Screen Size	C-10	C-11	Total	Cumulative	Percent	Screen Size	D-1	D-2	D-3	D-3a	D-4	D-5	D-6	D-7	D-8	D-9	D-9a	D-10	D-11	D-12	D-14	D-15	D-16	D-17	D-18
1-1/2-inch	0.025	0.770	1.500	21.912	100.00	1-1/2-inch	1.072	0.114	1.521	1.521	0.033	0.182	0.000	0.000	0.000	0.000	0.000	0.221	0.000	0.040	0.000	0.000	0.484	0.000	0.000
3/4-inch	0.616	0.287	1.591	20.412	93.15	3/4-inch	0.177	0.058	0.243	0.243	0.036	0.150	0.037	0.000	0.102	0.094	0.094	0.482	0.000	0.046	0.028	0.068	0.000	0.085	0.138
No. 4	0.904	0.847	4.299	18.821	85.89	No. 4	1.018	0.325	0.628	0.628	0.197	0.281	0.103	0.032	0.022	0.895	0.895	0.671	0.405	0.072	0.058	0.197	0.095	0.281	0.467
No. 8	---	---	---	---	---	No. 8	---	---	0.223	---	---	---	---	---	---	0.484	---	---	---	---	---	---	---	---	---
No. 10	0.482	0.735	2.231	14.522	66.27	No. 10	0.695	0.235	---	0.271	0.176	0.155	0.037	0.037	0.015	---	0.636	0.291	0.195	0.026	0.028	0.075	0.008	0.383	0.214
No. 16	---	---	---	---	---	No. 16	---	---	0.192	---	---	---	---	---	---	0.610	---	---	---	---	---	---	---	---	---
No. 200	3.354	1.528	10.444	12.291	56.09	No. 200	1.162	2.705	2.482	2.626	2.493	1.075	0.205	0.297	0.056	2.645	3.103	4.173	1.750	0.154	0.098	0.668	0.013	5.041	1.379
Passing No. 200	0.497	0.430	1.847	1.847	8.43	Passing No. 200	0.175	0.354	0.312	0.312	0.278	0.153	0.025	0.032	0.025	0.503	0.503	0.252	0.378	0.003	0.028	0.279	0.016	0.041	0.470
Total	5.878	4.597	21.912	---	---	Total	4.299	3.791	5.601	5.601	3.213	1.996	0.407	0.398	0.220	5.231	5.231	6.090	2.728	0.301	0.240	1.287	0.616	5.831	2.658

Ring D (Continued)						Ring E																	
Screen Size	D-19	D-20	Total	Cumulative	Percent	Screen Size	E-1	E-2	E-3	E-3a	E-4	E-4a	E-7	E-7a	E-8	E-9	E-9a	E-10	E-11	E-12	E-13	E-13a	E-14	E-14a	E-15
1-1/2-inch	0.198	0.000	3.825	50.478	100.00	1-1/2-inch	0.000	0.000	0.000	0.000	0.014	0.014	0.000	0.000	0.000	0.000	0.000	0.030	0.000	0.035	0.000	0.000	0.000	0.000	0.000
3/4-inch	0.056	0.051	1.851	46.653	92.42	3/4-inch	0.127	0.000	0.054	0.054	0.000	0.000	0.100	0.100	0.065	0.000	0.000	0.000	0.015	0.048	0.052	0.052	0.000	0.000	0.000
No. 4	0.440	0.321	6.508	44.802	88.76	No. 4	0.736	0.022	0.092	0.092	0.132	0.132	0.055	0.055	0.048	0.007	0.007	0.063	0.027	0.287	0.003	0.003	0.018	0.018	0.056
No. 8	---	---	---	---	---	No. 8	---	---	0.064	---	0.083	---	0.040	---	---	0.005	---	---	---	---	0.005	---	0.001	---	---
No. 10	0.300	0.262	4.039	38.294	75.86	No. 10	1.051	0.038	---	0.081	---	0.111	---	0.051	0.001	---	0.005	0.058	0.002	0.225	---	0.006	---	0.001	0.003
No. 16	---	---	---	---	---	No. 16	---	---	0.070	---	0.111	---	0.045	---	---	0.002	---	---	---	---	0.004	---	0.001	---	---
No. 200	1.665	1.691	30.354	34.255	67.86	No. 200	1.725	0.057	0.673	0.726	1.415	1.498	0.432	0.466	0.002	0.002	0.004	0.186	0.002	3.101	0.010	0.013	0.002	0.003	0.004
Passing No. 200	0.397	0.180	3.901	3.901	7.73	Passing No. 200	0.302	0.011	0.122	0.122	0.164	0.164	0.097	0.097	0.001	0.001	0.001	0.025	0.002	0.232	0.002	0.002	0.002	0.002	0.005
Total	3.056	2.505	50.478	---	---	Total	5.941	0.178	1.075	1.075	1.919	1.919	0.769	0.769	0.117	0.017	0.017	0.332	0.048	3.928	0.076	0.076	0.024	0.024	0.068

Ring E (Continued)																								
Screen Size	E-16	E-17	E-18	E-19	E-19a	E-20	E-21	E-21a	E-22	E-23	E-23a	E-24	E-24a	E-25	E-25a	E-26	E-26a	E-27	E-28	E-29	E-30	E-30a	Total	Cumulative	Percent
1-1/2-inch	0.000	0.000	0.000	0.000	0.000	0.000	0.000	0.000	0.000	0.000	0.000	0.305	0.305	0.303	0.303	0.005	0.005	0.000	0.068	0.065	0.000	0.000	0.795	17.994	100.00
3/4-inch	0.024	0.046	0.041	0.116	0.116	0.037	0.022	0.022	0.000	0.021	0.021	0.178	0.178	0.215	0.215	0.055	0.055	0.062	0.012	0.127	0.045	0.045	1.462	17.199	95.58
No. 4	0.081	0.032	0.010	0.075	0.075	0.071	0.063	0.063	0.048	0.121	0.121	0.079	0.079	0.093	0.093	0.034	0.034	0.031	0.092	0.178	0.245	0.245	2.849	15.737	87.46
No. 8	---	---	---	0.007	---	---	0.001	---	---	0.011	---	0.026	---	0.005	---	0.013	---	---	---	---	0.062	---	---	---	---
No. 10	0.001	0.000	0.000	---	0.008	0.007	---	0.001	0.003	---	0.012	---	0.031	---	0.006	---	0.014	0.001	0.111	0.025	---	0.068	1.921	12.888	71.62
No. 16	---	---	---	0.004	---	---	0.001	---	---	0.003	---	0.022	---	0.005	---	0.004	---	---	---	---	0.025	---	---	---	---
No. 200	0.001	0.001	0.003	0.015	0.018	0.003	0.001	0.002	0.002	0.020	0.022	0.119	0.136	0.075	0.079	0.043	0.046	0.005	1.405	0.071	0.075	0.094	9.675	10.967	60.95
Passing No. 200	0.001	0.001	0.002	0.005	0.005	0.002	0.001	0.001	0.002	0.020	0.020	0.072	0.072	0.025	0.025	0.030	0.030	0.003	0.081	0.036	0.045	0.045	1.292	1.292	7.18
Total	0.108	0.080	0.056	0.222	0.222	0.120	0.089	0.089	0.055	0.196	0.196	0.801	0.801	0.721	0.721	0.184	0.184	0.102	1.769	0.502	0.497	0.497	17.994	---	---

(Continued)

* "a" denotes adjustment to include No. 10.

TABLE 3.4 (Concluded)

	Ring F																											
Screen Size	F-1	F-1a	F-2	F-2a	F-3	F-3a	F-4	F-7	F-7a	F-8	F-8a	F-10	F-10a	F-11	F-12	F-12a	F-13	F-14	F-15	F-16	F-18	F-18a	F-19	F-19a	F-20	F-20a	F-21
1-1/2-inch	0.045	0.045	0.000	0.000	0.000	0.000	0.000	0.000	0.000	0.006	0.006	0.000	0.000	0.000	0.000	0.000	0.000	0.000	0.000	0.000	0.000	0.000	0.000	0.000	0.000	0.000	0.000
3/4-inch	0.033	0.033	0.000	0.000	0.055	0.055	0.000	0.000	0.000	0.000	0.000	0.000	0.000	0.000	0.057	0.057	0.067	0.060	0.023	0.000	0.000	0.000	0.000	0.000	0.000	0.000	0.000
No. 4	0.285	0.285	0.010	0.010	0.025	0.025	0.007	0.055	0.055	0.015	0.015	0.045	0.045	0.005	0.008	0.008	0.045	0.033	0.025	0.045	0.010	0.010	0.013	0.013	0.023	0.023	0.045
No. 8	0.475	---	0.002	---	0.003	---	---	0.072	---	0.005	---	0.006	---	---	0.004	---	---	---	---	---	0.006	---	0.003	---	0.003	---	---
No. 10	---	0.603	---	0.005	---	0.004	0.001	---	0.076	---	0.006	---	0.006	0.005	---	0.006	0.005	0.001	0.006	0.002	---	0.008	---	0.003	---	0.004	0.001
No. 16	0.512	---	0.012	---	0.003	---	---	0.015	---	0.005	---	0.001	---	---	0.008	---	---	---	---	---	0.008	---	0.002	---	0.005	---	---
No. 200	2.405	2.789	0.012	0.021	0.003	0.005	0.002	0.031	0.042	0.004	0.008	0.006	0.007	0.006	0.009	0.015	0.005	0.001	0.002	0.001	0.017	0.023	0.001	0.003	0.002	0.006	0.001
Passing No. 200	0.333	0.333	0.004	0.004	0.001	0.001	0.001	0.020	0.020	0.004	0.004	0.005	0.005	0.005	0.009	0.009	0.005	0.001	0.002	0.001	0.009	0.009	0.001	0.001	0.002	0.002	0.001
Total	4.088	4.088	0.040	0.040	0.090	0.090	0.011	0.193	0.193	0.039	0.039	0.063	0.063	0.021	0.095	0.095	0.127	0.096	0.058	0.049	0.050	0.050	0.020	0.020	0.035	0.035	0.048

	Ring F (Continued)																										
Screen Size	F-22	F-23	F-23a	F-25	F-25a	F-27	F-27a	F-28	F-28a	F-29	F-29a	F-30	F-30a	F-32	F-32a	F-33	F-33a	F-35	F-35a	F-36	F-36a	F-39	F-39a	F-40	F-40a	Total
1-1/2-inch	0.000	0.000	0.000	0.000	0.000	0.000	0.000	0.000	0.000	0.000	0.000	0.000	0.000	0.000	0.000	0.016	0.016	0.000	0.000	0.000	0.000	0.000	0.000	0.000	0.000	0.067
3/4-inch	0.012	0.010	0.010	0.000	0.000	0.006	0.006	0.025	0.025	0.000	0.000	0.000	0.000	0.021	0.021	0.000	0.000	0.000	0.000	0.031	0.031	0.000	0.000	0.000	0.000	0.400
No. 4	0.023	0.043	0.043	0.010	0.010	0.075	0.075	0.095	0.095	0.009	0.009	0.037	0.037	0.112	0.112	0.025	0.025	0.005	0.005	0.022	0.022	0.032	0.032	0.024	0.024	1.206
No. 8	---	0.001	---	0.003	---	0.003	---	0.002	---	0.005	---	0.001	---	0.025	---	0.007	---	0.003	---	0.003	---	0.002	---	0.020	---	---
No. 10	0.001	---	0.001	---	0.003	---	0.003	---	0.002	---	0.006	---	0.001	---	0.038	---	0.008	---	0.004	---	0.004	---	0.003	---	0.023	0.839
No. 16	---	0.002	---	0.002	---	0.001	---	0.002	---	0.006	---	0.002	---	0.052	---	0.005	---	0.005	---	0.003	---	0.004	---	0.013	---	---
No. 200	0.001	0.001	0.003	0.003	0.005	0.005	0.006	0.003	0.005	0.004	0.009	0.006	0.008	0.510	0.549	0.008	0.012	0.009	0.013	0.003	0.005	0.003	0.006	0.016	0.026	3.585
Passing No. 200	0.001	0.001	0.001	0.002	0.002	0.001	0.001	0.003	0.003	0.005	0.005	0.004	0.004	0.205	0.205	0.008	0.008	0.008	0.008	0.003	0.003	0.003	0.003	0.011	0.011	0.659
Total	0.038	0.058	0.058	0.020	0.020	0.091	0.091	0.130	0.130	0.029	0.029	0.050	0.050	0.925	0.945	0.069	0.069	0.030	0.030	0.065	0.065	0.044	0.044	0.084	0.084	6.756

Ring F (Continued)			Ring G															
Screen Size	Cumulative	Percent	Screen Size	G-32	G-32a	G-40	G-40a	G-42	G-42a	G-44	G-44a	G-55	G-59	Total	Cumulative	Percent
1-1/2-inch	6.756	100.00	1-1/2-inch	0.100	0.100	0.000	0.000	0.000	0.000	0.000	0.000	0.000	0.000	0.100	0.223	100.00
3/4-inch	6.689	99.01	3/4-inch	0.020	0.020	0.000	0.000	0.000	0.000	0.000	0.000	0.000	0.000	0.020	0.123	55.16
No. 4	6.289	93.09	No. 4	0.012	0.012	0.001	0.001	0.012	0.012	0.000	0.000	0.015	0.015	0.055	0.103	46.19
No. 8	---	---	No. 8	0.002	---	0.001	---	0.002	---	0.013	---	---	---	---	---	---
No. 10	5.083	75.24	No. 10	---	0.002	---	0.001	---	0.002	---	0.014	0.003	0.001	0.023	0.048	21.52
No. 16	---	---	No. 16	0.002	---	0.001	---	0.002	---	0.004	---	---	---	---	---	---
No. 200	4.244	62.82	No. 200	0.002	0.004	0.001	0.002	0.001	0.003	0.003	0.006	0.002	0.001	0.018	0.025	11.21
Passing No. 200	0.659	9.75	Passing No. 200	0.002	0.002	0.001	0.001	0.001	0.001	0.003	0.003	0.000	0.000	0.007	0.007	3.14
Total	---	---	Total	0.140	0.140	0.005	0.005	0.018	0.018	0.023	0.023	0.020	0.017	0.223	---	---

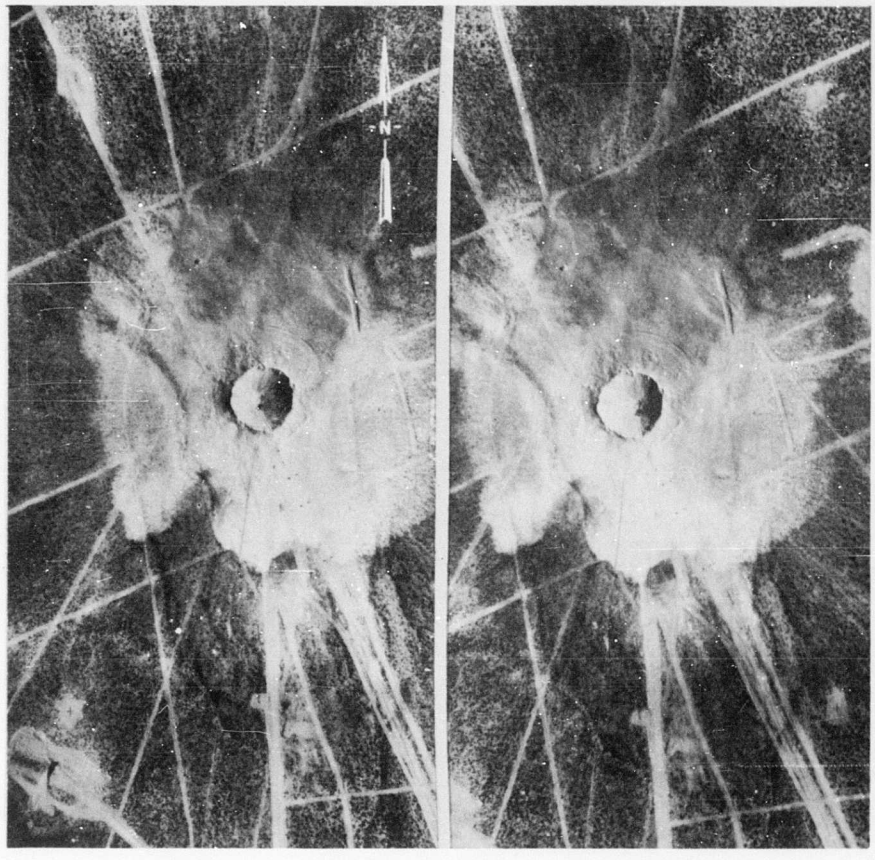

Figure 3.1 Aerial stereopair of the Johnie Boy crater, showing the lip and general pattern of ejecta distribution. For three-dimensional effect, use standard stereoscope.

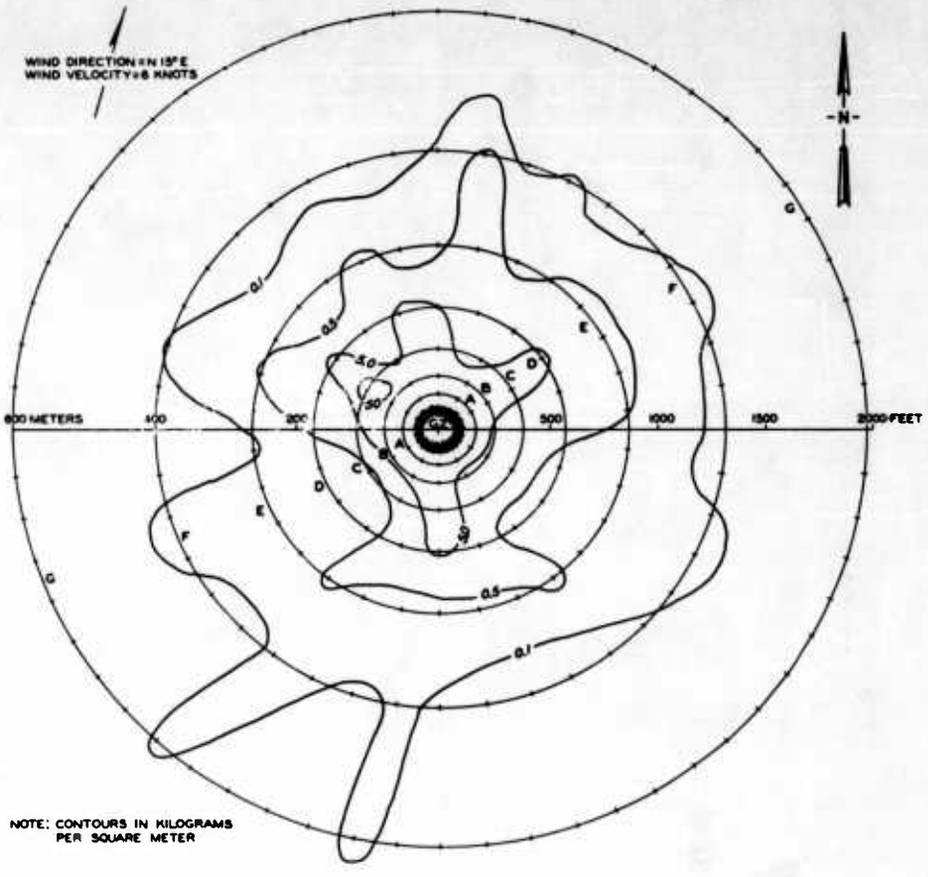

Figure 3.2 Ejecta distribution contours.

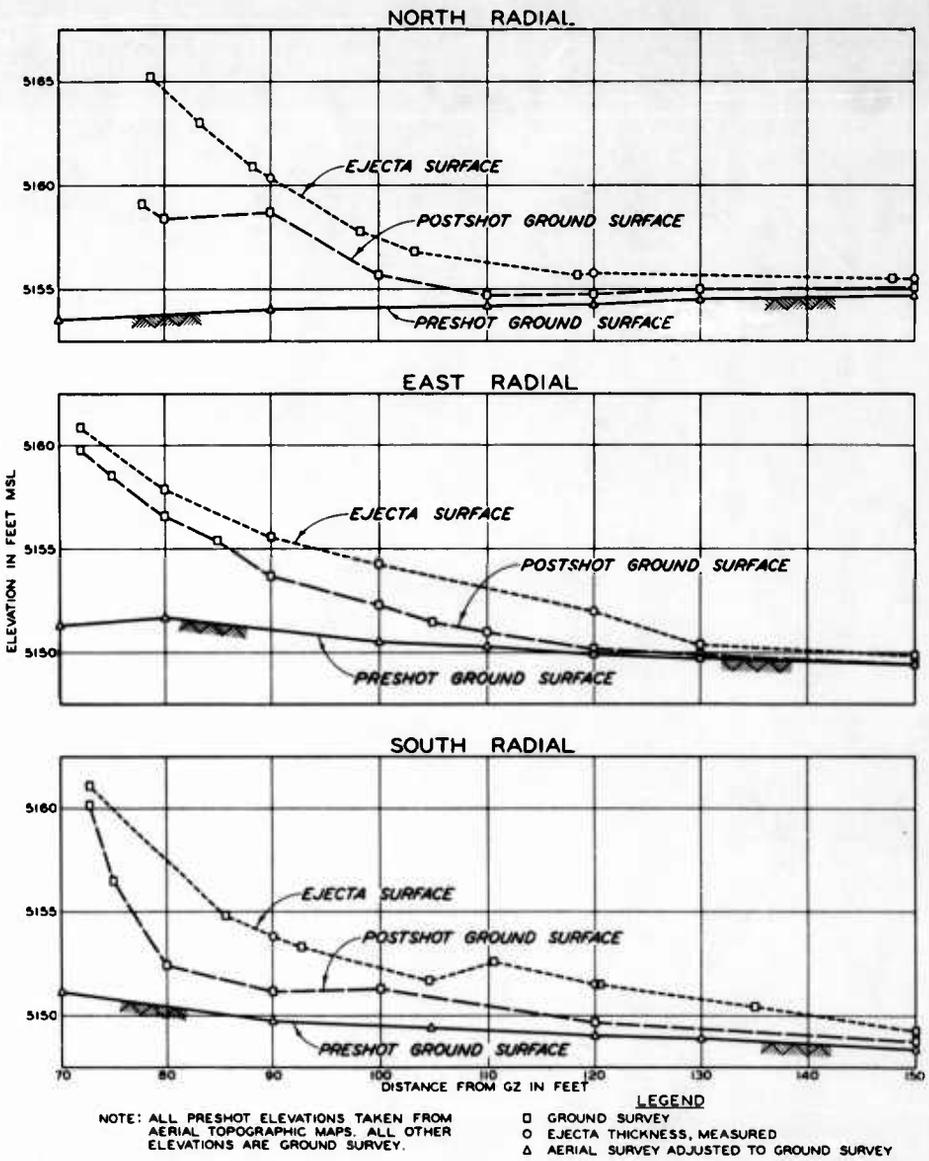

Figure 3.3 Crater lip profiles.

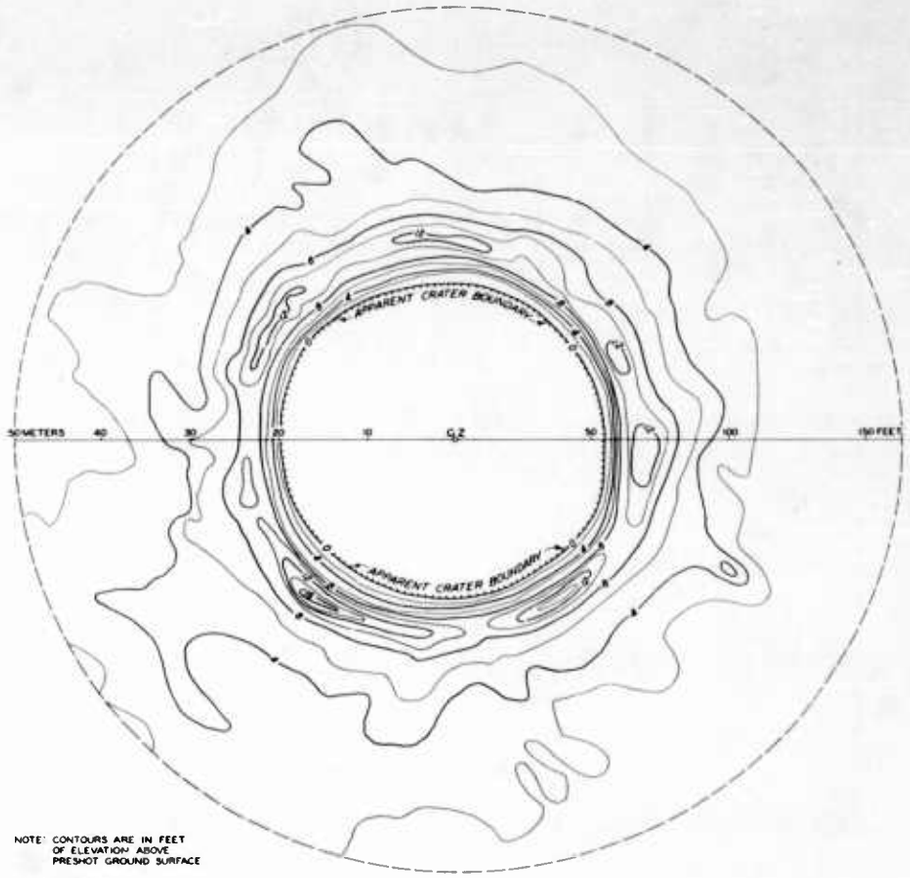

Figure 3.4 Postshot ejecta surface elevations reduced to a horizontal reference plane.

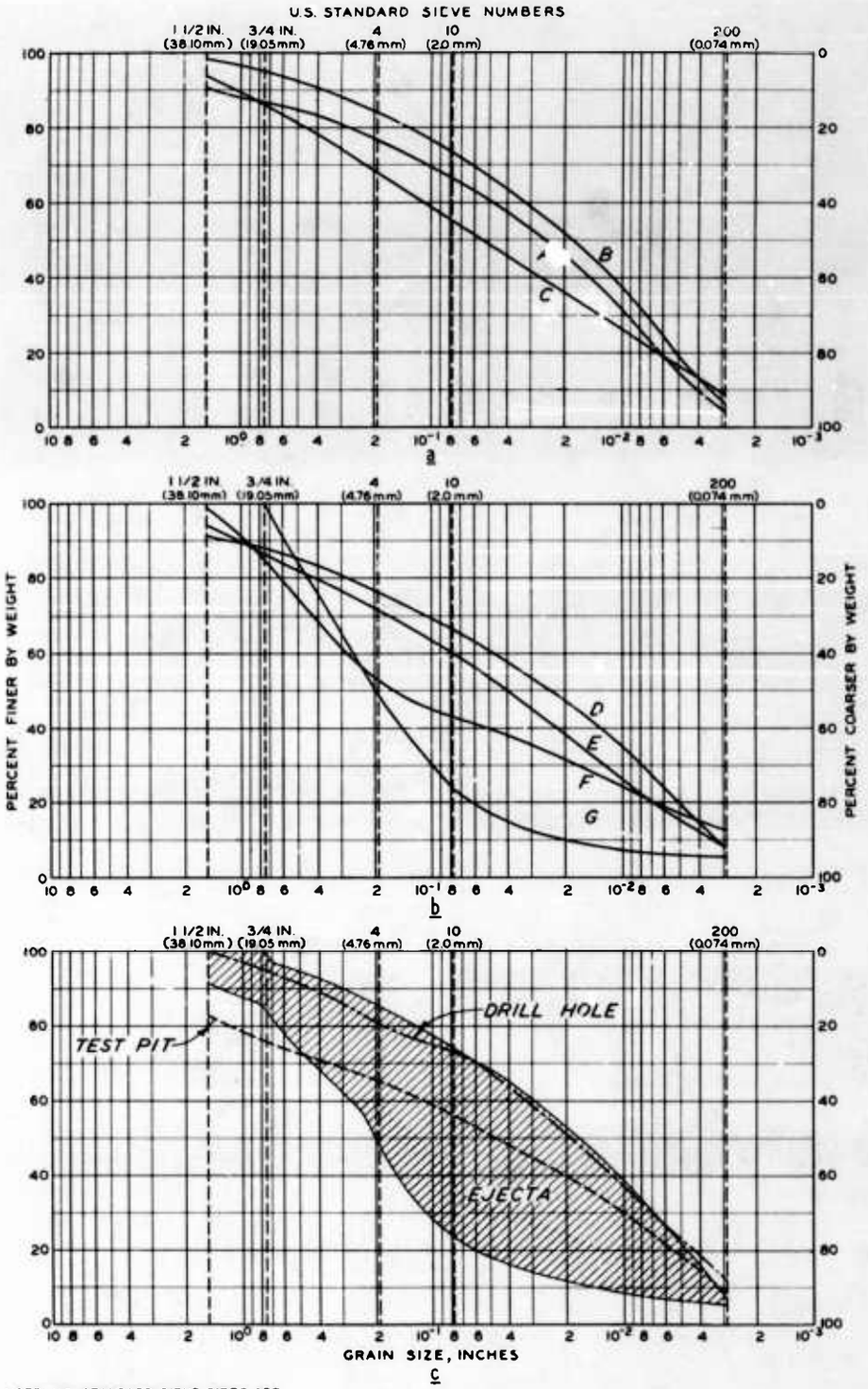

NOTE: U.S. STANDARD SIEVE SIZES ARE SHOWN BY DASHED LINES.
SAMPLES F-1 AND G-32 ARE NOT INCLUDED.

Figure 3.5 In situ and collector ring cumulative particle size distributions.

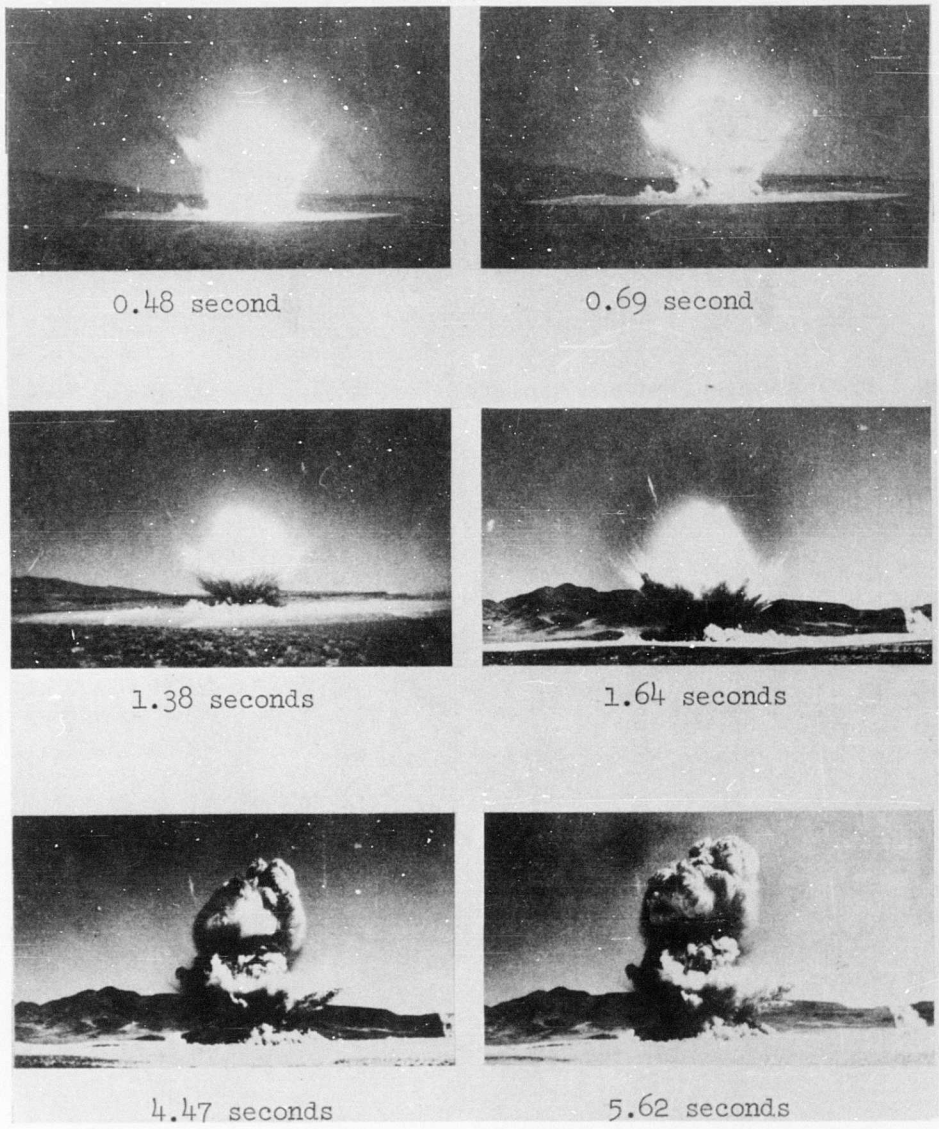

Figure 3.6 Sequence of selected EG&G photographs of Johnie Boy, showing fireball and ejecta at designated times after detonation.

CHAPTER 4

DISCUSSION

4.1 RELIABILITY OF DATA

4.1.1 General. Within the scope of its planned objectives, the Johnie Boy Project 1.5 provided adequate information for an accurate representation of the ejecta distribution except perhaps for large particle sizes. For the purposes of engineering analysis, and considering budgetary limitations, sample collectors were placed in maximum numbers and sizes. A layout designed to yield sufficient data for rigorous statistical and mathematical treatment would have increased costs considerably. The Johnie Boy ejecta study utilized 186 sampling stations, as compared, for example, with 272 for the Sedan study. Thus, in relation to the size (yield) of the test shot, the Johnie Boy throwout study represents one of the most detailed projects of its kind conducted to date.

The close-in samples could not, because of objectionable radiation levels, be collected until several weeks after the event, and the amount of fine material in each of these samples was unquestionably affected by wind and

precipitation; however, the amount deposited or removed by winds was considered to be negligible percentagewise. No attempt was made to control the moisture content of the samples during processing; however, in the arid climate of Nevada, this is probably of minor importance. A few samples were wet when recovered, but these dried out before final processing was begun.

The question of identification of ejecta should also be considered. Near the crater edge, overturning and apparent sliding of bedding planes accounted for most of the lip height. Overturned planes could be readily identified, principally by their inverted root systems, and were treated as ejecta. Sliding of the planes was more difficult to detect, and these sections were not considered ejecta, although it is recognized that they contributed to the crater volume. Farther from GZ, there were found on some collectors particles too large to be attributed to postshot deposition by wind, and yet, by their low radiation levels, apparently not from the crater. It seems likely that air turbulence accompanying the blast caused these depositions by merely blowing or rolling particles along the ground from one point to another. There seemed to be no practical way

of separating particles according to their origin, so all were treated as ejecta.

4.1.2 Statistical Considerations. For possible theoretical/statistical treatment, the deposited ejecta mass may be considered as a population composed of particles of varying sizes at increasing distances from GZ. The statistical parameters are weight per unit area, distance from GZ, and particle size distribution. Closely related factors are the particle size distribution of the in situ alluvium and the drag effects of the air on particle trajectories. Even when it is assumed that the detonation produces considerable fragmenting of in situ particles, the extent of which would be difficult to evaluate, the in situ distribution is believed to be closely related to that of the ejecta.

Although the collector array for Johnie Boy was symmetrical with respect to GZ, for statistical purposes it may be assumed that a random sampling of ejecta was obtained. In the planning of experiments of this type, there is no way to predict the circumferential variation of ejecta deposition, and a symmetrical collector array is therefore best suited to obtain a random, representative group of samples. In order that these samples be equally representative, it is

desirable that those on a given ring be of approximately the same weight. This is particularly necessary where an arithmetical average is involved. As mentioned in Section 3.2, two samples were not included in the averages for outer rings because of their excessive weights.

4.2 PARTICLE SIZE DISTRIBUTION

Particle size distributions by ring (Figure 4.1) depict graphically the sorting that results from trajectory mechanics in air. The amounts of all large material (No. 10 and above) except +1-1/2-inch increased in proportion to the distance traveled. Although the larger size particles represent a fairly large portion of the in situ alluvium, their percentage distribution by number is small. It can readily be shown that the area covered by the collectors in the outer rings was so small compared to the few large particles propelled to these distances that the probability of one of them landing upon a collector was remote. Truly representative sampling would have required collectors with total areas varying in proportion to distances from GZ; thus, taking the collectors on ring A as standard, the G ring would have required a sampling area of more than 100 m^2,

or 144 individual collectors. Using this criterion for the entire sampling array would have required approximately 400 collectors. Thus a modified procedure based on the above criterion was employed by which a convenient collector size was made the standard, and the numbers of collectors were varied so as to provide a sampling array that was economically manageable within the funds provided for the study.

If the number of particles per unit weight of material rather than weight only is considered, together with the fact that a one-cubic-inch particle is equal to 1,000 1/10th-inch particles and is also equal to 4.03×10^7 particles of minus No. 200 mesh size, it is readily seen why the weight percentage of larger particles may be much too low for samples obtained at the greater ranges where small, uniform-size collectors are employed. Thus, while the +3/4-inch material increases out to 400 meters, there was (except for sample G-32) none of this size ejecta found on the collectors at 600 meters. It can be reasoned, therefore, that sampling such as used in this experiment did not give a true measure of the amount of coarse material which was actually ejected to the distances at which the collectors were placed. The sorting indicated did, however, give

a qualitative indication of the effects of air drag in determining the distances to which ejecta will travel, both where the trajectories are completely ballistic and where the settling occurs at terminal velocities.

Particles in the size range less than 2 mm will quickly reach terminal velocities lower than 1 m/sec and would be expected to fall near the crater if there were no wind. Since the 7-mph wind recorded for the Johnie Boy event had no discernible effect on the deposition pattern, a large part of the minus No. 200 material found upon the collectors in the outer rings must have been deposited by the base surge or by the later effects of weather.

Figure 4.2, which gives the settling velocities of quartz in air, shows that fragments larger than 100 to 200 mm might not be accelerated enough by the explosion to reach terminal velocities and would therefore behave ballistically. Because of their high terminal velocities (caused by a low drag force/mass ratio), fragments above 2 mm in diameter could be expected to be projected to much greater ranges compared to smaller particles. In still air, particles finer than 0.1 mm settle so slowly that any turbulence in the air would tend to keep them airborne, and by

this means they could be transported some distance from the crater.

With the present limited knowledge on this subject, it would be difficult to apply the equations for trajectories of particles in air (Appendix B), largely because of the uncertainties concerning initial velocities and air drag. Also, the quantitative effects of the expanding gas bubble and the blast wind on ejecta distribution are not known. A final, meaningful evaluation of ejecta parameters will require utilization of equations of the type given in Appendix B and an extension of the theory of trajectories and the mechanics of motion of both large and small particles in air.

4.3 DISTRIBUTION OF EJECTA

The manner in which ejecta is deposited upon the ground surface per unit area (δ , kg/m^2) as the result of a surface or underground explosion is dependent upon: (1) the yield or equivalent weight of explosive, (2) the depth (position) at which the explosion occurs, and (3) the characteristics of the medium cratered (Reference 10). There are other factors that influence to a relatively minor degree the amount

and pattern of throwout, e.g. wind conditions, type of explosive (which in turn determines the energy-coupling characteristics of the explosion), inhomogeneities within the medium itself, etc. Until more data are available from a variety of nuclear explosions in a variety of materials, the problem may well be simplified to

$$\delta (R) = f (W, Z, \sigma) \qquad (4.1)$$

where $\delta (R)$ is a functional relation between the deposition per unit area and R, the range from GZ; W is the yield (weight of explosive); Z is the scaled position of the charge with reference to the air-ground interface; and σ is the strength properties of the medium cratered. For the Johnie Boy shot, W, Z, and σ are simply parameters of the experiment; hence, the deposition per unit area depends mainly upon the range from GZ, or

$$\delta = f (R) \qquad (4.2)$$

The observed pattern of ejecta deposition for Johnie Boy is shown by means of a contoured map in Figure 3.2. In general, the Johnie Boy distribution pattern conforms to those obtained from similar experiments conducted under

similar weather conditions. For Johnie Boy, quantities of ejecta deposition per unit area large enough to be of concern as an overburden problem (say 5 kg/m^2, or approximately 1 lb/ft^2) generally occurred within a radial distance of less than 200 meters, or within about 10 apparent crater radii of GZ.

In Figure 4.3, ejecta distribution for Johnie Boy is plotted logarithmically as a function of radial distance from GZ. Average values of ejecta thicknesses were employed with an assumed specific gravity of 1.5 to calculate the ejecta mass (weight) inside the 50-meter ring, while the mean values of ejecta weights on recoverable collectors were used to determine ejecta distribution at radial distances corresponding to collector rings (Table 4.1). The total mass of ejecta, M_e, was then calculated from the equation

$$M_e = 2\pi \int_{R_o}^{\infty} \delta (R)\, R\, dR \qquad (4.3)$$

where $\delta (R)$ is the equation of the curve shown in Figure 4.3 as determined by the method of least squares. The Johnie Boy ejecta data are thus described by

$$\delta = 2.06 \times 10^8 R^{-3.65} \qquad (4.4)$$

The mass (weight) of ejecta between the lip crest and infinity was determined from Equations 4.3 and 4.4 to be approximately 4.45×10^6 kg.

4.4 EJECTA EQUATIONS

The results of a number of ejecta studies are summarized in Appendix A. In each case, the amount of ejecta deposited per unit area is expressed by an equation of the form of Equation 4.4, or

$$\delta = k R^m \qquad (4.5)$$

where k is a constant for a given set of data, R is the radial distance from GZ in meters, and m is the slope (characteristically negative) of the curve assuming a straight line on logarithmic paper.

There is some question as to the total applicability of an equation of the form of Equation 4.5. For example, if the Johnie Boy ejecta data are plotted on semilogarithmic paper, the plot in Figure 4.4 results. This plot indicates that there are two regimes of exponential behavior. One regime applies over the range from the peak of the crater lip, which occurs at a distance of about 23 meters from GZ, out to approximately 50 meters. The second regime applies

over the interval from about 50 meters out to the most distant station from which ejecta was reccvered, or at least 600 meters.

The superiority of one system of graphical presentation of the data over the other (compare Figures 4.3 and 4.4) is not clearly established. While the data appear to fit a hyperbolic formulation equally well, there are theoretical suggestions that an exponential formulation would be more appropriate, e.g. Newton's law of cooling, which represents quite well almost any phenomenon that gradually diminishes, as does the thickness of throwout deposition.

In order to compare Johnie Boy ejecta results with results of other studies, a hyperbolic formulation is used in this report. Future work in this field should examine in more detail the exponential approach, particularly as regards the two or more regimes of behavior. An extensive effort to further develop this approach at this time is not possible because data are not available in sufficient detail.

4.5 PREDICTION OF EJECTA DEPOSITION

The ejecta equations presented in Table A.1 (Appendix A) can be transposed to the dimensionless form

(Reference 10) and written as follows:

$$\frac{\delta\, r_a\, d_a}{W} = b\left(\frac{R}{r_a}\right)^m \qquad (4.6)$$

Solution for the coefficient b yields the following:

$$\frac{k\, R^m\, r_a\, d_a}{W} \cdot \frac{r_a^{\,m}}{R^m} = b$$

$$b = \frac{k\, r_a^{\,1+m}\, d_a}{W} \qquad (4.7)$$

Table 4.2 presents the transposed ejecta equations (in dimensionless form) for specific shots in desert alluvium. Figures 4.5 and 4.6 provide plots of these equations. If the Stagecoach II curve is omitted, primarily because of its abnormal slope, the characteristic slope shown in Figure 4.6 represents the average slope of all remaining curves. In effect, this assumes that the characteristic slope for ejecta curves in desert alluvium can be adequately represented by a function

$$\frac{\delta\, r_a\, d_a}{W} = b\left(\frac{R}{r_a}\right)^{-3.4} \qquad (4.8)$$

Such a supposition presumes that the factor b is a function of the depth of the explosion. Figure 4.7 presents a

plot of b versus scaled depth of burst, Z' . The correlation appears to be adequate for both HE and NE charges. Stagecoach II again was omitted from the plot for the reason stated above.

Ejecta deposition can be thus predicted for a wide variety of depths of burst by using Figure 4.7 in conjunction with Equation 4.8 and the predicted apparent crater radius and depth.

4.6 RELATIVE DISTRIBUTION OF EJECTA

The fraction of total ejecta volume (dimensionless) as a function of range from GZ in units of crater radii is shown in Figure 4.8. The Johnie Boy shot fits well within the envelope of data established by previous HE and NE shots in desert alluvium. Figure 4.8 shows that 53 percent of the Johnie Boy ejecta was deposited within two crater radii from GZ, 75 percent within three crater radii, and approximately 90 percent within five crater radii. Thus, most of the ejecta is deposited within ranges wherein only hardened facilities will be expected to survive.

An equation for estimating the thickness of ejecta deposition (t_e) for various explosion yields in desert

alluvium (surface or near-surface burst) can be developed as follows. Since the ejecta deposition δ (kg/m^2) can be defined as

$$\delta = c \left(\frac{R}{r_a} \right)^m \tag{4.9}$$

and the ejecta thickness can be determined by dividing δ by the specific weight (density) of the material, it follows that

$$\frac{\delta}{\gamma} = t_e$$

or

$$t_e = \frac{c}{\gamma} \left(\frac{R}{r_a} \right)^m \tag{4.10}$$

The scaled ejecta thickness is then defined by

$$\frac{t_e}{W^{1/3.4}} = \frac{c}{\gamma W^{1/3.4}} \left(\frac{R}{r_a} \right)^m \tag{4.11}$$

Using the ejecta data for Jangle HE-2 and for Johnie Boy (tabulated with that for other desert alluvium shots in Table 4.3), Equation 4.11 becomes

$$t_e = 5.3 \times 10^{-2} W^{1/3.4} \left(\frac{R}{r_a} \right)^{-3.4} \tag{4.12}$$

Equation 4.12 is applicable to surface (or very near

surface) explosions in desert alluvium and can be used for estimating the ejecta thickness in meters.

4.7 RELATION BETWEEN EJECTA VOLUME AND CRATER VOLUME

A correlation between the total volume of ejecta (V_e) and the apparent crater volume (V_a) for various shots in desert alluvium is shown in Table 4.4 and Figure 4.9. The relation is satisfactorily described by

$$V_e = k_1 V_a^n \tag{4.13}$$

where k_1 is a constant and n an exponent. Since the exponent of V_a in Equation 4.13 is less than 1, the ratio V_e/V_a decreases as V_a becomes larger, indicating that the volume within the apparent crater attributable to compression and plastic flow increases as the apparent volume increases but not in direct proportion.

If the volume due to gross compression and plastic flow is considered to be equal to the apparent crater volume less the total ejecta volume, then

$$V_{cf} = V_a - V_e$$

or

$$V_{cf} = V_a - k_1 V_a^n \tag{4.14}$$

Thus, Equation 4.14 provides a general expression for estimating the crater volume that is due to compression and plastic flow of the medium cratered.

TABLE 4.1 AVERAGE EJECTA DATA FOR JOHNIE BOY

Station	R, Radial Distance from GZ	δ, Weight of Ejecta per Unit Area	$\frac{\delta\, r_a\, d_a}{W}$*	$\frac{R}{r_a}$
	meters	kg/m^2		
Lip	24.4	1,890	7.24×10^{-1}	1.31
Lip	27.4	537	2.06×10^{-1}	1.47
Lip	36.6	350	1.34×10^{-1}	1.97
Lip	45.7	231	8.84×10^{-2}	2.46
Ring A	50	13.3	5.09×10^{-3}	2.69
Ring B	75	10.7	4.10×10^{-3}	4.03
Ring C	115	8.37	3.22×10^{-3}	6.18
Ring D	175	2.52	9.62×10^{-4}	9.41
Ring E	265	0.39	1.49×10^{-4}	14.3
Ring F	400	0.11	4.21×10^{-5}	21.5
Ring G	600	0.004	1.53×10^{-6}	32.2

* r_a = 18.6 meters, d_a = 9.3 meters, and W = 4.53×10^5 kg

TABLE 4.2 A LISTING OF EJECTA EQUATIONS FOR VARIOUS SHOTS IN DESERT ALLUVIUM

Event	Scaled Depth of Burst, Z'	Dimensionless Form of the Ejecta Equation
	$ft/kt^{1/3.4}$	
Johnie Boy	2.4	$\frac{\delta r_a d_a}{W} = 1.86 \left(\frac{R}{r_a} \right)^{-3.65}$
Jangle HE-2	16	$\frac{\delta r_a d_a}{W} = 5.18 \left(\frac{R}{r_a} \right)^{-3.37}$
ERA 108	18	$\frac{\delta r_a d_a}{W} = 5.10 \left(\frac{R}{r_a} \right)^{-2.71}$
ERA 112	50	$\frac{\delta r_a d_a}{W} = 69.7 \left(\frac{R}{r_a} \right)^{-3.75}$
Stagecoach II	54	$\frac{\delta r_a d_a}{W} = 1.45 \left(\frac{R}{r_a} \right)^{-2.46}$
ERA 115	55	$\frac{\delta r_a d_a}{W} = 8.85 \left(\frac{R}{r_a} \right)^{-3.17}$
Teapot Ess	64	$\frac{\delta r_a d_a}{W} = 75.2 \left(\frac{R}{r_a} \right)^{-3.94}$
Stagecoach III	108	$\frac{\delta r_a d_a}{W} = 35.8 \left(\frac{R}{r_a} \right)^{-3.39}$
Scooter	153	$\frac{\delta r_a d_a}{W} = 5.85 \left(\frac{R}{r_a} \right)^{-3.30}$
Sedan	164	$\frac{\delta r_a d_a}{W} = 5.55 \left(\frac{R}{r_a} \right)^{-3.64}$

TABLE 4.3 EJECTA EQUATIONS FOR EXPLOSIONS AT SIMILAR SCALED DEPTHS OF BURSTS IN DESERT ALLUVIUM

Event	Explosive	Yield, W	δ - Ejecta Distribution, kg/m^2	
		kg	kR^m	$c(R/r_a)^m$
Near-Surface Bursts				
Jangle HE-2	HE	1.81×10^4	$7.6 \times 10^6 R^{-3.37}$	$1.71 \times 10^3 (R/r_a)^{-3.37}$
Johnie Boy	NE	4.53×10^5	$2.06 \times 10^8 R^{-3.65}$	$4.77 \times 10^3 (R/r_a)^{-3.65}$
Depths of Burst ~ 65 $ft/kt^{1/3}$				
Teapot Ess	NE	1.1×10^6	$2.1 \times 10^{11} R^{-3.94}$	$6.85 \times 10^4 (R/r_a)^{-3.94}$
Stagecoach II	HE	1.81×10^4	$1.95 \times 10^5 R^{-2.46}$	$2.34 \times 10^2 (R/r_a)^{-2.46}$
ERA 112	HE	1.16×10^3	$9.46 \times 10^6 R^{-3.75}$	$2.40 \times 10^3 (R/r_a)^{-3.75}$
ERA 115	HE	1.81×10^4	$2.05 \times 10^7 R^{-3.17}$	$1.0 \times 10^3 (R/r_a)^{-3.17}$
Depths of Burst ~ 150 $ft/kt^{1/3}$				
Sedan	NE	9.1×10^7	$5.77 \times 10^{12} R^{-3.64}$	$2.54 \times 10^4 (R/r_a)^{-3.64}$
Scooter	HE	4.5×10^5	$7.95 \times 10^8 R^{-3.30}$	$2.46 \times 10^3 (R/r_a)^{-3.30}$
Stagecoach III	HE	1.81×10^4	$7.32 \times 10^7 R^{-3.39}$	$4.24 \times 10^3 (R/r_a)^{-3.39}$

TABLE 4.4 APPARENT CRATER VOLUME AND EJECTA DATA FOR SHOTS IN DESERT ALLUVIUM AND DRY SAND*

	Event	W	Depth of Burst	Z'	V_a		M_a	V_e**		M_e
		kt	ft	$ft/kt^{1/3.4}$	ft^3	m^3	kt	ft^3	m^3	kt
1.	ERA 108	1.28×10^{-3}	2.6	18	5.2×10^{3}	1.5×10^{2}	2.78×10^{-1}	1.91×10^{3}	5.41×10^{1}	8.93×10^{-2}
2.	ERA 112	1.28×10^{-3}	7.0	50	1.3×10^{4}	3.7×10^{2}	6.50×10^{-1}	1.21×10^{4}	3.43×10^{2}	5.66×10^{-1}
3.	ERA 115	2.00×10^{-2}	17.5	55	1.8×10^{5}	5.1×10^{3}	9.31	5.50×10^{4}	1.56×10^{3}	2.57
4.	Jangle HE-2	2.00×10^{-2}	5.13	16	3.5×10^{4}	9.9×10^{2}	1.78	2.29×10^{4}	6.48×10^{2}	1.07
5.	Stagecoach II	2.00×10^{-2}	17.1	54	8.36×10^{4}	2.37×10^{3}	4.16	7.28×10^{4}	2.06×10^{3}	3.64
6.	Stagecoach III	2.00×10^{-2}	34.2	108	1.45×10^{5}	4.11×10^{3}	7.20	1.13×10^{5}	3.20×10^{3}	5.30
7.	Scooter	5.00×10^{-1}	125.0	153	2.64×10^{6}	7.48×10^{4}	1.34×10^{2}	4.87×10^{5}	1.38×10^{4}	2.28×10^{1}
8.	Johnie Boy	5×10^{-1}	1.92	2.4	1.45×10^{5}	4.11×10^{3}	8.35	1.05×10^{5}	2.97×10^{3}	4.91
9.	Teapot Ess	1.2	67	64	2.6×10^{6}	7.4×10^{4}	1.32×10^{2}	1.21×10^{6}	3.43×10^{4}	5.65×10^{1}
10.	Sedan	100	635	164	1.79×10^{8}	5.07×10^{6}	9.1×10^{3}	9.73×10^{7}	2.76×10^{6}	4.55×10^{3}

* Source material: References 1 and 8.
** Assumed density = 1.5 gm/cm^3

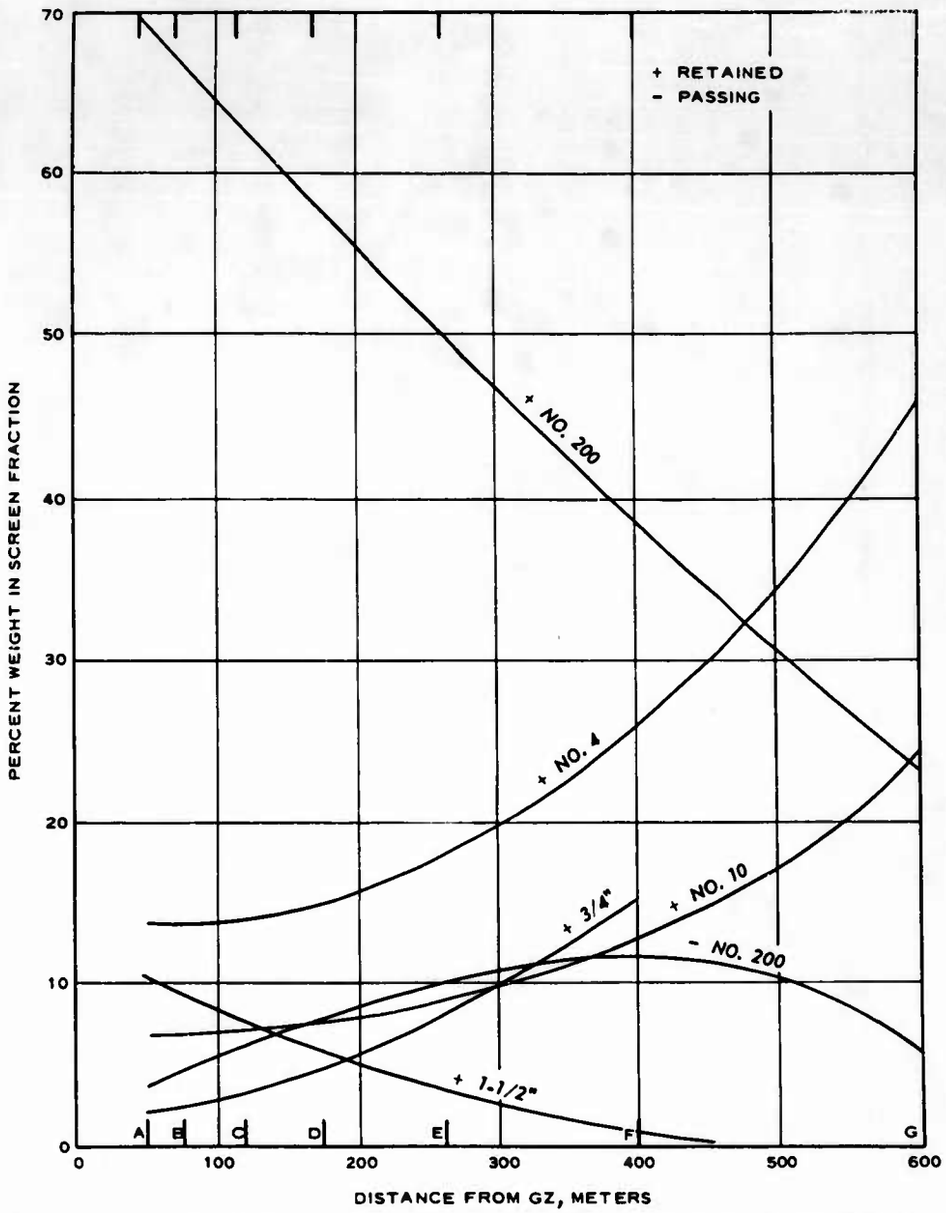

Figure 4.1 Variation of screen size fractions with distance from GZ. Note ring designations on abscissa. Samples F-1 and G-32 are not considered in this graph.

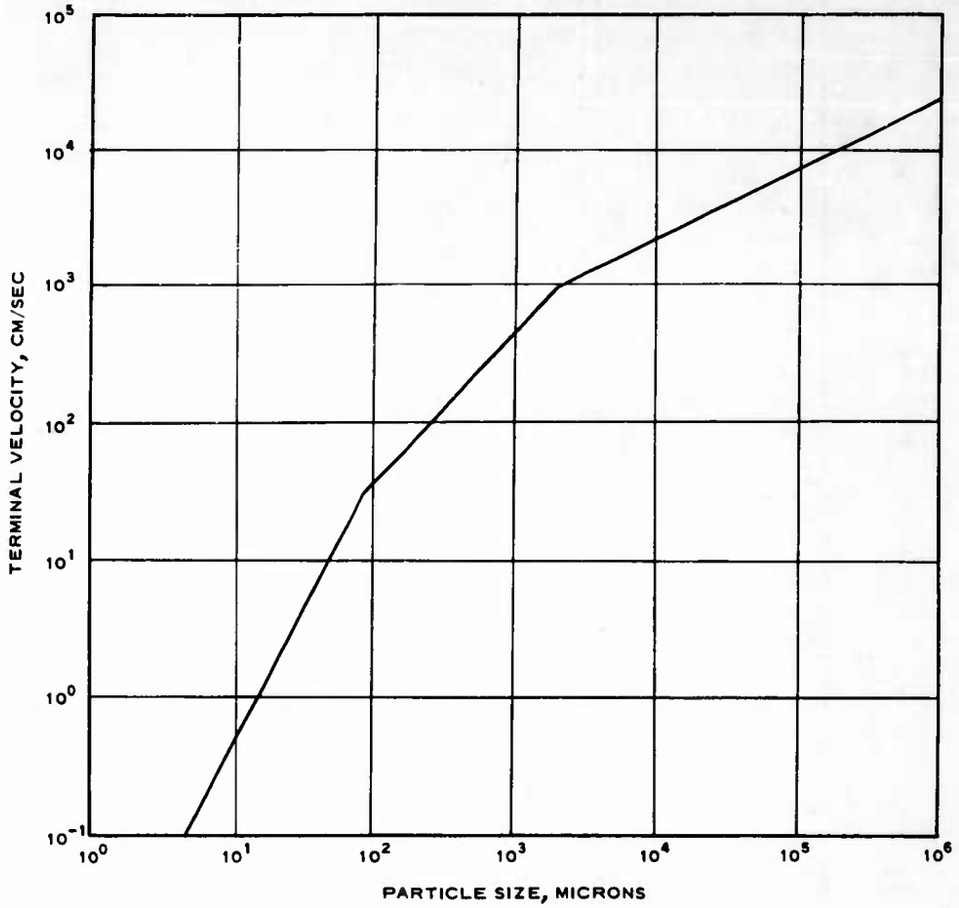

Figure 4.2 Settling velocities of quartz in air (Reference 15).

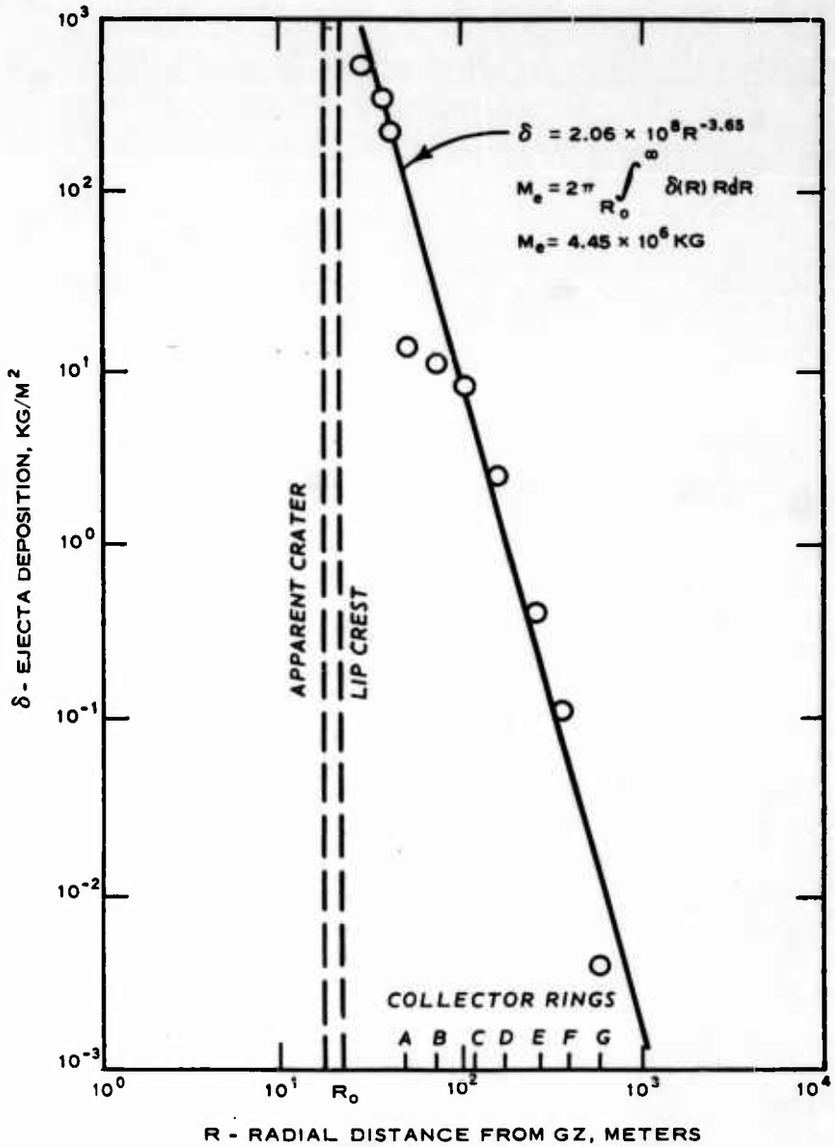

Figure 4.3 Ejecta distribution, Johnie Boy. Data points represent arithmetic means of recoverable samples. One data point, 1,890 kg/m^2 at 24.4 meters, is not shown. Data points for rings A and B were not used in computation of curve.

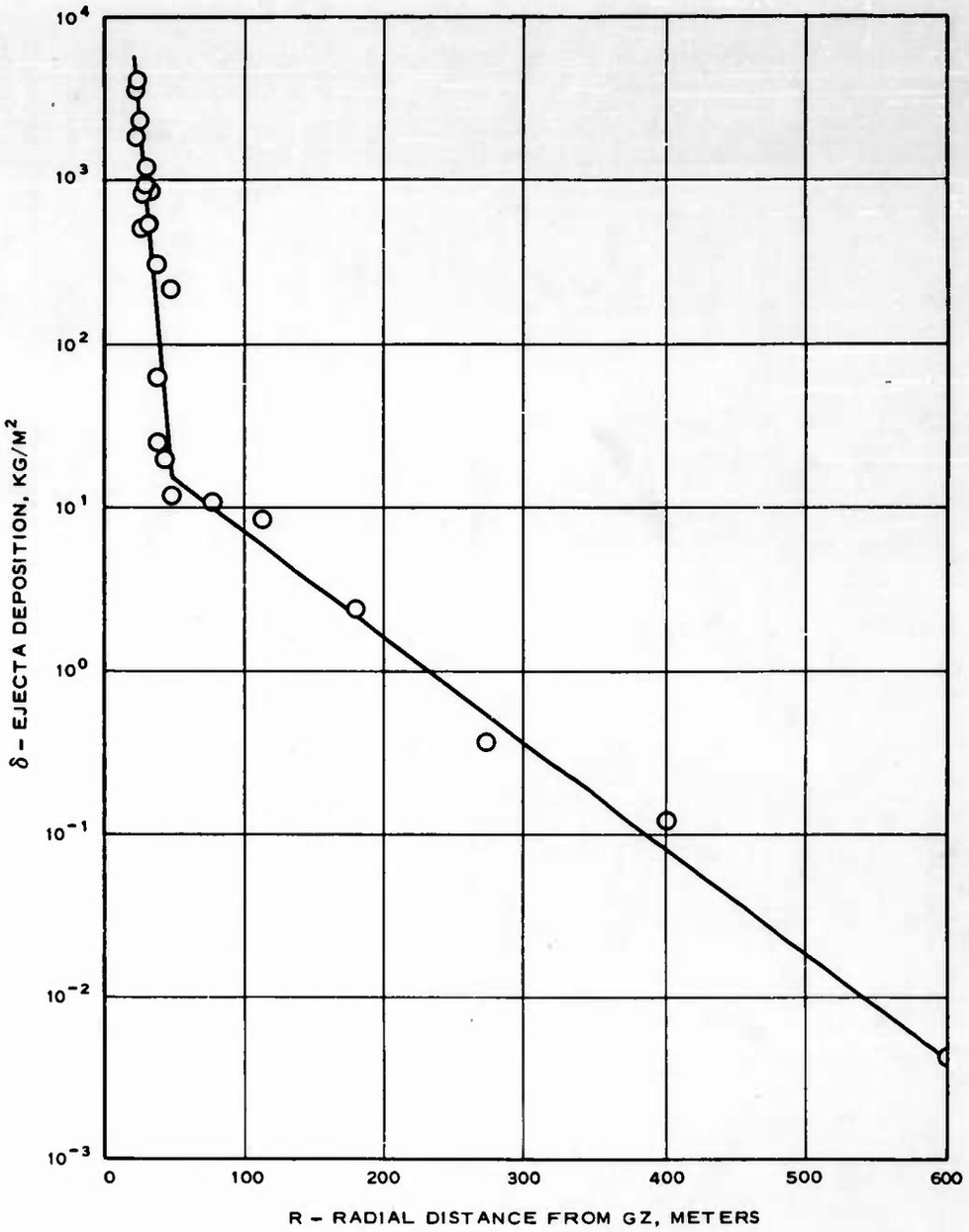

Figure 4.4 Exponential distribution of ejecta, Johnie Boy.

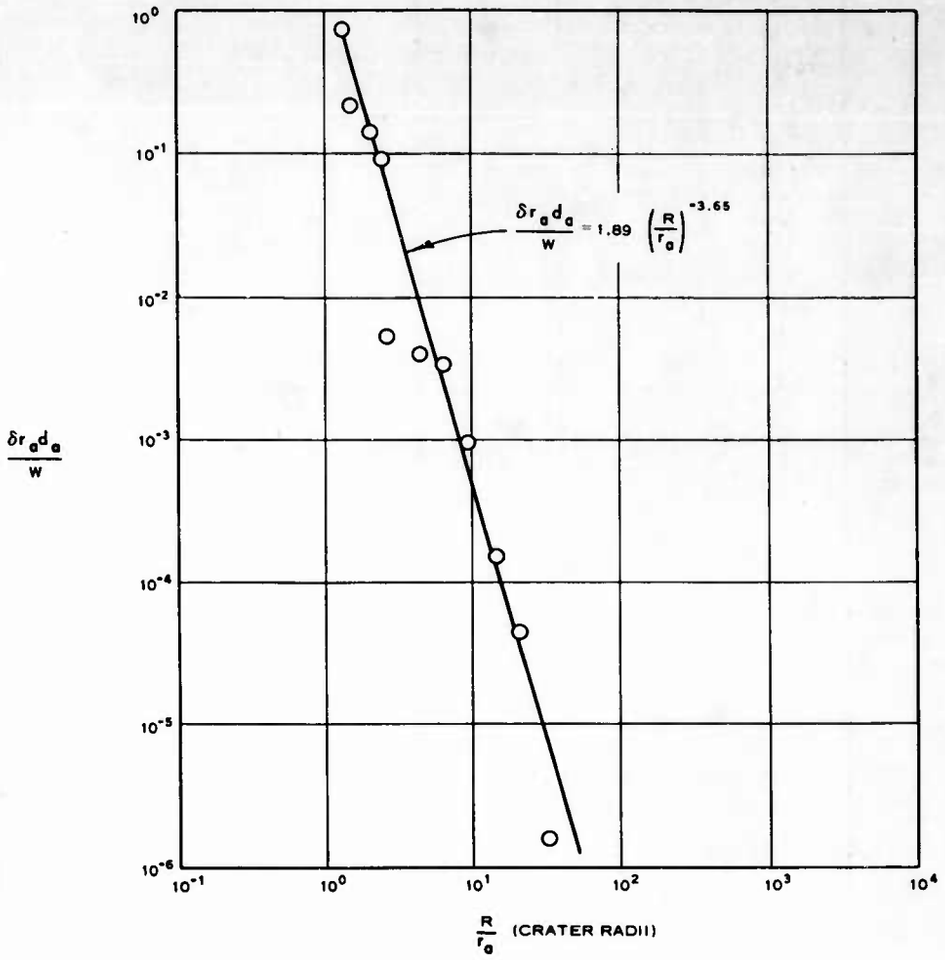

Figure 4.5 Dimensionless plot of ejecta deposition versus range for Johnie Boy.

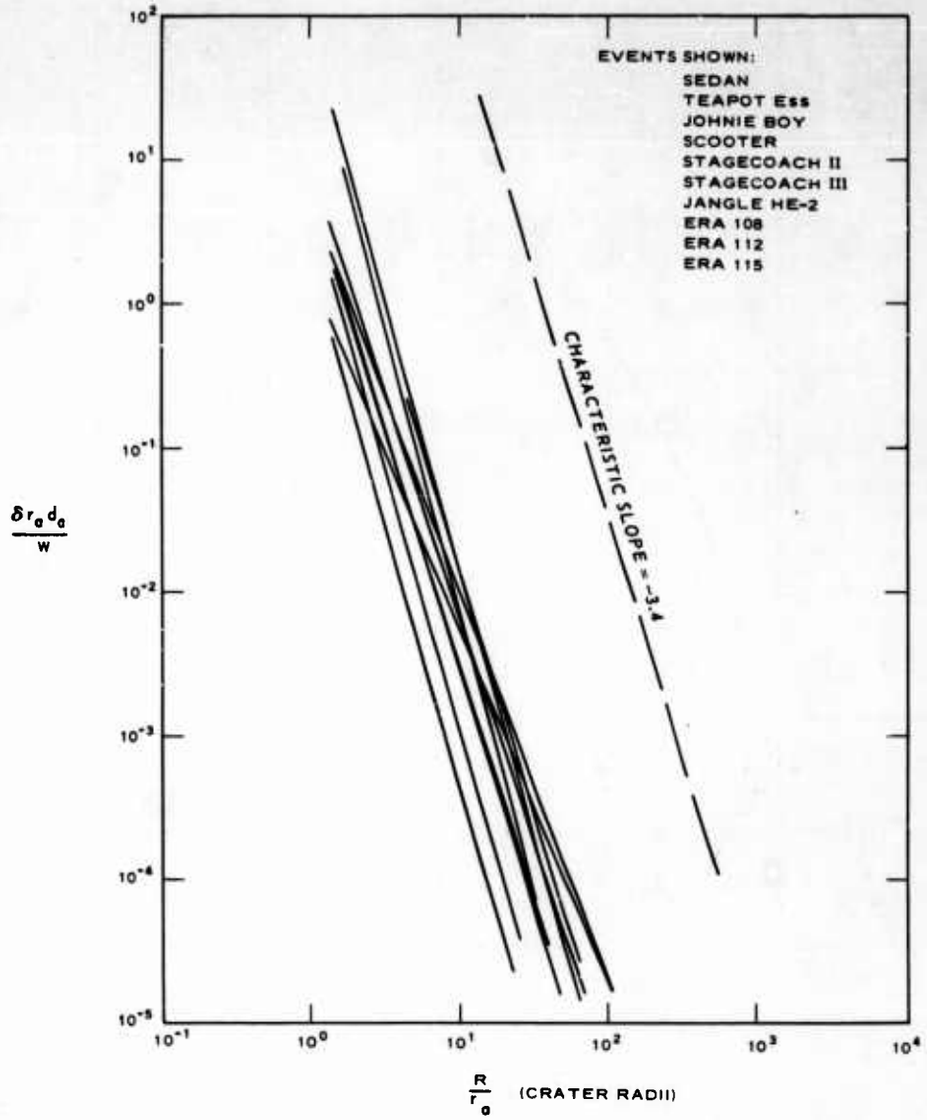

Figure 4.6 Dimensionless plot of ejecta equations shown in Table 4.2.

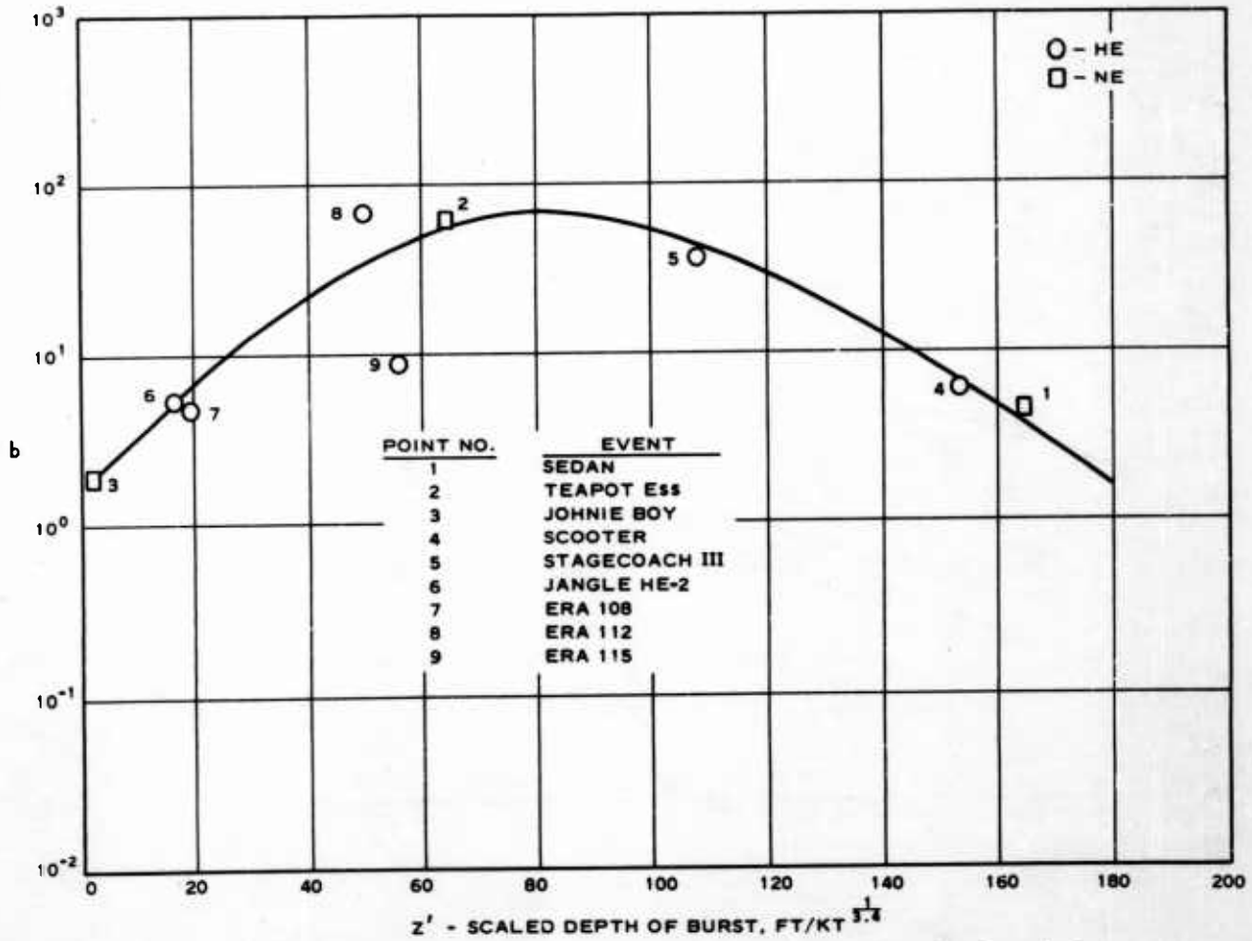

Figure 4.7 Variation of b with scaled depth of burst for shots in desert alluvium.

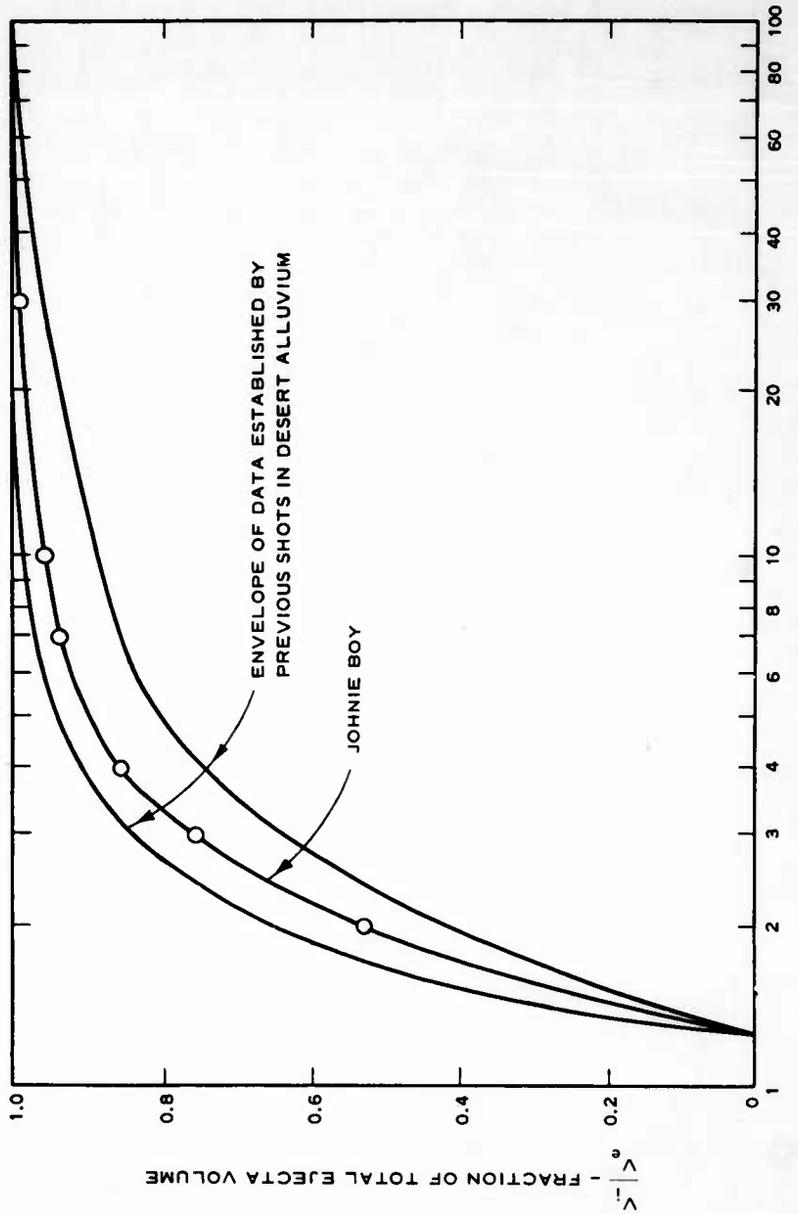

Figure 4.8 Fraction of total ejecta volume as a function of range from GZ. Envelope is from Reference 2.

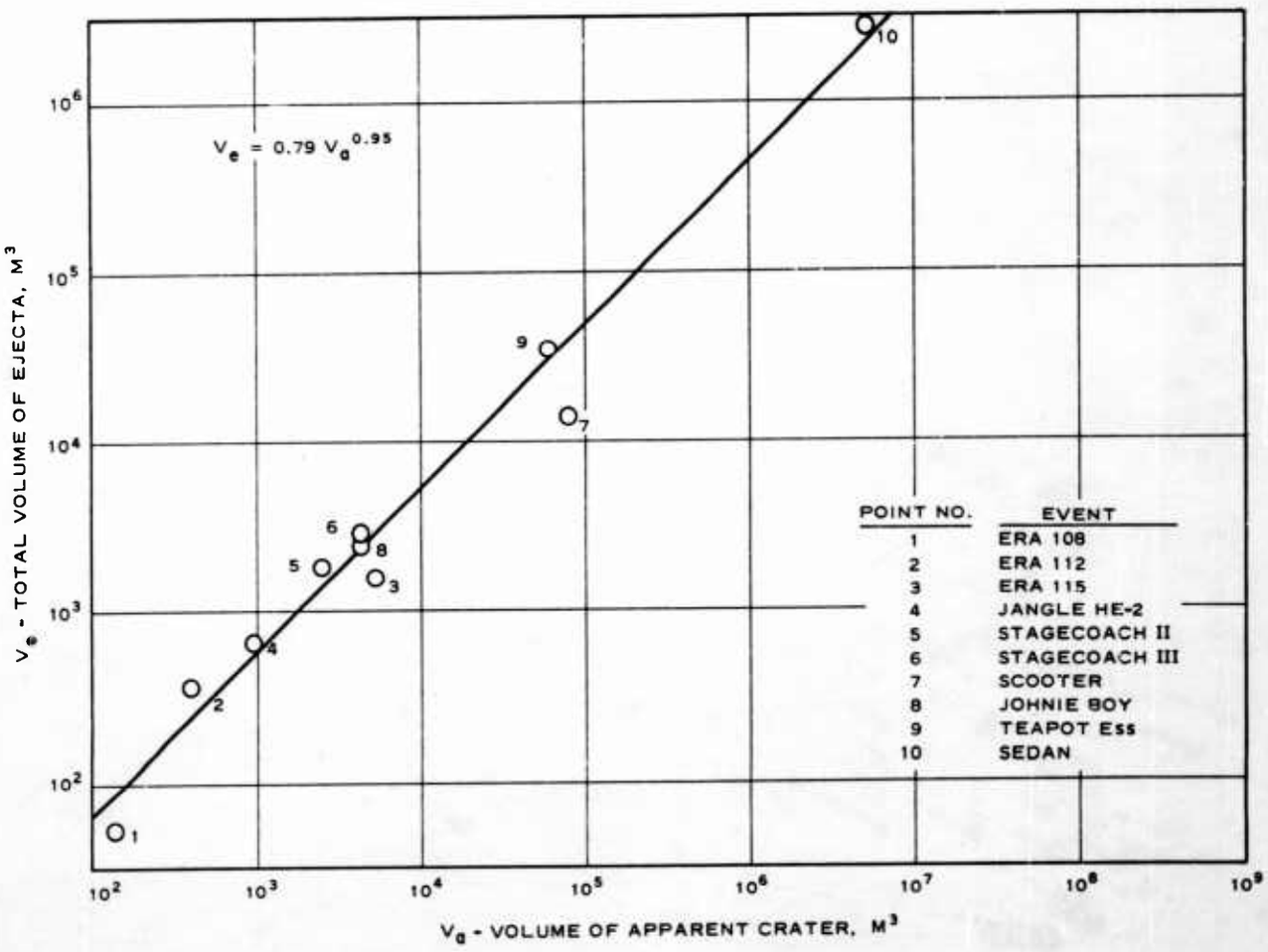

Figure 4.9 Variation of apparent crater volume with total volume of ejecta for various shots in desert alluvium.

CHAPTER 5

CONCLUSIONS AND RECOMMENDATIONS

5.1 CONCLUSIONS

The Brode mathematical model (Reference 11) appears to serve quite well as a qualitative explanation of the movement of material from craters in alluvium, although it was derived to apply to tuff.

A straight-line, logarithmic plot of δ versus R appears to give a good representation of ejecta distribution between the crest of the crater lip and the outer limit to which throwout is a problem as such (i.e. excluding fallout). This treatment also provides a means of comparing the various ejecta studies that have been conducted to date.

Within the range of yields for which experience is available in ejecta studies, prediction of throwout is feasible by the methods developed in Chapter 4. For desert alluvium, 90 percent or more of all ejecta can be expected to fall within 10 crater radii of GZ. The Johnie Boy shot, which should closely approximate a low-yield, tactical ground burst, indicates that throwout should not be an overburden problem to hardened military installations beyond this distance.

Particle size analysis showed that there was considerable sorting of ejecta by air drag, the percentage of material finer than screen size No. 10 decreasing rapidly with distance from GZ. Much of the finest material, especially minus No. 200, is believed to have been deposited by the base surge or by postshot weather. Wind did not influence that part of the ejecta which would constitute an overburden problem.

In Johnie Boy Project 1.5, a relatively simple experiment provided good data on and a better insight into the problem of nuclear surface bursts, such as might be expected in the tactical employment of nuclear weapons. The experimental technique herein reported, including both sample collection and close-in excavation, may be improved by experience and more adequate funding.

5.2 RECOMMENDATIONS

Prediction of throwout phenomena for extremely large yields will require additional experimentation. Also, refinement of the knowledge gained thus far in this field is desirable. For these purposes, full advantage should be taken of large-scale explosive testing, especially shallow

HE and NE bursts in the kt range and similarly positioned NE bursts in the Mt range.

A better technique of ejecta sampling is desirable. In addition to the use of collectors for fine particles and excavation through the crater lip to define close-in ejecta, the preshot spraying of areas beyond the predicted crater lip with a colored, cohesive paint is suggested. In conjunction with some sort of a coordinate system, this should permit the taking (or simply measuring in place) of many more ejecta samples, or more important, of larger samples at greater distances, which would give a more accurate representation of ejecta distribution and total mass.

Future ejecta studies should include a consideration of an exponential formulation, as discussed in Chapter 4, and should, if possible, define the regimes characterizing throwout behavior.

Finally, the initiation of a program to establish mathematical models for trajectories of ejecta with varying particle size distributions, and taking into account air drag and wind velocities, is also recommended.

APPENDIX A

SUMMARY OF CRATERING-EJECTA EXPERIMENTS

Table A.1 summarizes all usable cratering-ejecta experiments known to have been conducted to date, including Johnie Boy.

TABLE A.1 CRATER EJECTA STUDIES

Shot Designation or Event	Yield		Depth of Burst	Z'	d_a	d_t	r_a	r_t	V_a	V_t	Ejecta Distribution Equation	Cratered Material
	Kilotons (kt) or Tons (T)	kg	m	$m/kg^{1/3}$	m	m	m	m	m^3	m^3	kg/m^2	
NE												
Sedan	100 kt	9.1×10^7	193	0.43	97	--	195		5.07×10^6	--	$5.77 \times 10^{12} R^{-3.64}$	Desert alluvium
Teapot Ess	1.2 kt	1.1×10^6	20.3	0.20	27.4	--	44.4		7.36×10^4	--	$2.1 \times 10^{11} R^{-3.94}$	Desert alluvium
Danny Boy	0.42 kt	4.26×10^5	33.5	0.45	19.2	43.5	32.6		3.06×10^4	--	$5.69 \times 10^{18} R^{-8.55}$	Basalt
Johnie Boy	0.50 kt	4.53×10^5	0.6	0.01	9.3	--	18.6		4.09×10^3	--	$2.06 \times 10^8 R^{-3.65}$*	Desert alluvium
HE												
Scooter	0.5 kt	4.5×10^5	38	0.50	22.8	--	46.6	--	7.4×10^4	--	$7.95 \times 10^8 R^{-3.30}$	Desert alluvium
Stagecoach II	20 T	1.8×10^4	5.2	0.20	7.2	--	15.4	--	2.37×10^3	--	$1.95 \times 10^5 R^{-2.46}$	Desert alluvium
Stagecoach III	20 T	1.8×10^4	10.4	0.40	8.6	--	17.8	--	4.11×10^3	--	$7.32 \times 10^7 R^{-3.39}$	Desert alluvium
Suffield	5 T	4.5×10^3	Contact	~0.0	3.8	--	6.1	--	--	--	$4.5 \times 10^4 R^{-2.93}$	Silt and clay
Suffield	100 T	9.1×10^4	Contact	~0.0	6.2	--	23.5	--	3.55×10^3	--	$2.56 \times 10^8 R^{-3.65}$	Silt and clay
White Tribe I-III	6 T	5.2×10^3	Contact	~0.0	2.5	--	5.3	--	--	--	$8.9 \times 10^4 R^{-2.73}$	Caliche
Jangle HE-2	20 T	1.8×10^4	1.6	0.05	4.5	--	12.1	--	9.91×10^2	--	$7.6 \times 10^6 R^{-3.37}$	Desert alluvium
Buckboard (11)	20 T	1.8×10^4	7.8	0.30	7.6	--	13.6	--	1.53×10^3	--	$2.42 \times 10^5 R^{-2.36}$	Basalt
Buckboard (12)	20 T	1.8×10^4	13.0	0.50	10.6	--	17.4	--	3.82×10^3	--	$1.35 \times 10^6 R^{-2.68}$	Basalt
Buckboard (13)	20 T	1.8×10^4	17.9	0.68	4.9	--	11.2	--	6.56×10^2	--	$3.88 \times 10^5 R^{-2.86}$	Basalt
ERA 803	0.033 T	1.45×10^2	0.8	0.15	--	1.5	--	3.5	--	2.26×10^1	$2.21 \times 10^2 R^{-2.01}$	Sandstone
ERA 807	0.033 T	1.45×10^2	0.8	0.15	--	1.6	--	4.4	--	4.13×10^1	$6.23 \times 10^1 R^{-1.43}$	Sandstone
ERA 808	0.033 T	1.45×10^2	0.8	0.15	--	1.8	--	4.0	--	2.89×10^1	$7.02 \times 10^3 R^{-2.74}$	Sandstone
ERA 819	0.033 T	1.45×10^2	0.8	0.15	--	2.0	--	4.8	--	4.07×10^1	$2.60 \times 10^3 R^{-2.39}$	Sandstone
ERA 804	0.033 T	1.45×10^2	1.5	0.29	--	2.3	--	4.3	--	4.07×10^1	$1.51 \times 10^2 R^{-1.65}$	Sandstone
ERA 805	0.033 T	1.45×10^2	3.8	0.72	--	4.5	--	2.8	--	3.37×10^1	$3.20 \times 10^3 R^{-2.45}$	Sandstone
ERA 810	1.28 T	1.16×10^3	1.5	0.14	--	3.0	--	9.9	--	2.44×10^2	$8.83 \times 10^7 R^{-3.99}$	Sandstone
ERA 811	1.28 T	1.16×10^3	1.5	0.14	--	3.2	--	7.7	--	1.99×10^2	$2.71 \times 10^5 R^{-2.98}$	Sandstone
ERA 814	20 T	1.8×10^4	3.8	0.14	--	8.2	--	17.2	--	3.06×10^3	$3.59 \times 10^6 R^{-2.88}$	Sandstone
ERA 815	20 T	1.8×10^4	3.8	0.14	--	8.2	--	21.5	--	3.54×10^3	$6.10 \times 10^5 R^{-2.56}$	Sandstone
ERA 817	160 T	1.45×10^5	7.6	0.10	--	14.3	--	28.9	--	1.45×10^4	$1.51 \times 10^9 R^{-3.35}$	Sandstone
ERA 501	0.03 T	1.45×10^2	2.0	0.40	--	2.8	--	3.4	--	7.25×10^1	$5.94 \times 10^2 R^{-1.84}$	Limestone
ERA 110	0.16 T	1.45×10^2	1.1	0.21	2.3	2.7	4.0	5.1	4.53×10^2	7.92×10^1	$3.83 \times 10^2 R^{-1.98}$	Dry sand
ERA 108	1.28 T	1.16×10^3	0.8	0.10	3.0	3.2	5.8	8.2	1.47×10^2	3.11×10^2	$3.64 \times 10^4 R^{-2.71}$	Dry sand
ERA 112	1.28 T	1.16×10^3	2.1	0.20	3.7	5.3	9.1	10.3	3.68×10^2	7.08×10^2	$9.46 \times 10^6 R^{-3.75}$	Dry sand
ERA 115	20 T	1.81×10^4	5.4	0.21	7.0	9.1	22.9	25.2	5.91×10^3	8.49×10^3	$2.05 \times 10^7 R^{-3.17}$	Dry sand
ERA 316	0.03 T	5.0×10	0.7	0.20	1.8	--	2.7	--	2.09×10^1	--	$4.98 \times 10^2 R^{-2.18}$	Dry clay
ERA 304	0.16 T	1.45×10^2	1.1	0.20	1.8	3.1	3.2	4.2	2.32×10^1	8.78×10^1	$7.45 \times 10^4 R^{-3.36}$	Dry clay
ERA 310	0.16 T	1.45×10^2	1.1	0.20	2.1	3.1	3.4	4.4	2.54×10^1	8.21×10^1	$1.10 \times 10^5 R^{-3.37}$	Dry clay
ERA 313	0.16 T	1.45×10^2	1.1	0.20	2.4	2.9	3.9	4.7	4.25×10^1	8.50×10^1	$2.40 \times 10^3 R^{-2.27}$	Dry clay
ERA 305	0.16 T	1.45×10^2	2.1	0.40	2.1	3.5	3.6	5.0	3.68×10^1	1.30×10^2	$4.35 \times 10^5 R^{-3.69}$	Dry clay
ERA Symmetry	0.16 T	1.45×10^2	2.1	0.40	2.1	3.2	3.8	4.6	3.68×10^1	9.90×10^1	$4.02 \times 10^4 R^{-3.00}$	Dry clay
ERA 308	1.28 T	1.16×10^3	0.8	0.10	3.7	4.1	6.1	7.5	1.52×10^2	2.83×10^2	$1.22 \times 10^4 R^{-2.56}$	Dry clay
ERA 309	1.28 T	1.16×10^3	2.1	0.40	4.7	5.3	6.6	9.0	2.04×10^2	5.38×10^2	$1.12 \times 10^6 R^{-3.51}$	Dry clay
ERA 312	1.28 T	1.16×10^3	2.1	0.40	4.6	5.5	7.9	9.3	3.68×10^2	7.08×10^2	$1.12 \times 10^4 R^{-2.14}$	Dry clay
ERA 315	20 T	1.81×10^4	5.3	0.40	12.8	14.3	19.5	23.8	5.36×10^2	9.90×10^3	$1.62 \times 10^8 R^{-3.59}$	Dry clay
ERA 318	160 T	1.45×10^5	10.7	0.2	18.3	23.5	36.6	39.6	3.12×10^4	5.10×10^4	$9.91 \times 10^7 R^{-3.03}$	Dry clay
ERA 402	0.16 T	1.45×10^2	0.8	0.15	3.0	--	5.7	7.2	1.16×10^2	--	$5.51 \times 10^2 R^{-1.84}$	Wet clay
ERA 404	0.16 T	1.45×10^2	0.8	0.15	3.5	--	5.3	7.3	1.10×10^2	--	$1.12 \times 10^4 R^{-2.32}$	Wet clay
ERA 403	1.28 T	1.16×10^3	1.5	0.15	3.9	--	12.7	13.8	8.20×10^2	--	$7.15 \times 10^6 R^{-3.40}$	Wet clay

* Combined Boeing Airplane Co. and Sandia Corp. data.

APPENDIX B*

PARTICLE TRAJECTORIES

B.1 TRAJECTORIES IN A VACUUM

The well-known parametric equations for the parabolic trajectory of a projectile in a gravitational field, neglecting the effects of the atmosphere, are as follows:

$$x = v_o\, t \sin \theta_o \tag{B.1}$$

$$y = v_o\, t \cos \theta_o - \tfrac{1}{2} g\, t^2 \tag{B.2}$$

Figure B.1 illustrates these equations. Eliminating t and solving the resulting expression for v_o give v_o as a function of x, y, and θ_o. If an observed pair of values $x = R_p$ and $y = h$ are inserted, v_o as a function of θ_o is given by

$$v_o = \frac{R_p\, g^{1/2}}{(R_p \sin 2\theta_o - 2h \sin^2 \theta_o)^{1/2}} \tag{B.3}$$

If two different pairs of observed values of x and y are inserted, two independent equations which uniquely define v_o and θ_o result.

---

* Prepared by G. B. Clark and T. J. Kinzer, Jr., during their summer employment at WES, 1963.

B.2 DRAG ON PARTICLES IN A FLUID

As soon as a medium is introduced, drag forces should be considered. The treatment given this phenomenon is governed by the physical problem being considered. Given an airplane of known design, the question concerns the details of airflow around it at any velocity. The problem here is the distribution of throwout from an explosion. Even if the exact aerodynamic behavior of some given particle could be predicted (and it cannot), the details would be useless in view of the great variety of particle shapes which comprise the ejecta. Thus the simple approach by which the assumption is made that the ejecta may be characterized by certain empirical parameters inserted into the theory for drag on a sphere is an acceptable step toward producing some sort of distribution function.

If temperature effects are considered to be restricted to density effects, the drag on a sphere should depend upon its size and velocity and on the density and viscosity of the medium. Dimensional homogeneity then gives

$$D = \kappa\, d^{n}\, \mu^{2-n}\, \rho_{o}^{\,n-1}\, v^{n} \qquad \text{(B.4)}$$

If this is to be applied to arbitrary particles, the

parameters K and n must be known. The parameter K can be considered as depending upon the particle shape; n depends upon velocity, but fortunately it usually varies slowly. Conventionally, the streamline (laminar) flow regime is associated with $n = 1$ and the turbulent regime with $n = 2$. These values will be used here. It should be noted, however, that the drag on a projectile at high speed is not exactly proportional to v^2 (Reference 16). In the intermediate regime, the flow breaks away from the particle and changes considerably. In this regime, n can be less than one, and equations using $n = 2/3$ will be shown here to characterize this region. In fact, n varies continuously, and in the cases of very high Reynolds numbers ($\geq 5 \times 10^5$), there are velocities at which a small increase in v actually reduces drag.

The form of the equations of motion for each of these values of n will be given. Their derivation follows.

Let the position of a particle be specified by

$$\vec{r} = \vec{i}\, x + \vec{j}\, y + \vec{k}\, z \qquad \text{(B.5)}$$

in the coordinate system shown in Figure B.2. Let its velocity with respect to the ground be

$$\vec{u} = \dot{\vec{r}} = \vec{i}\, \dot{x} + \vec{j}\, \dot{y} + \vec{k}\, \dot{z} \qquad \text{(B.6)}$$

Then its acceleration with respect to the ground is

$$\vec{u} = \ddot{\vec{r}} = \vec{i}\,\ddot{x} + \vec{j}\,\ddot{y} + \vec{k}\,\ddot{z} \tag{B.7}$$

Assume that a constant horizontal wind of velocity $\vec{V}_w$ blows at an angle α with respect to the z-axis, i.e. in the $\phi = \alpha$ direction. The components of the wind are

$$\vec{V}_w = (V_w \sin\alpha)\,\vec{i} + (V_w \cos\alpha)\,\vec{k} \tag{B.8}$$

The drag force is determined by the particle velocity $\vec{v}$ with respect to the air, however, not the ground, and this velocity is

$$\vec{v} = \vec{u} - \vec{V}_w \tag{B.9}$$

Since drag is opposite in direction from particle velocity, the drag force can be written as

$$\begin{aligned}\vec{D} &= -\kappa\, d^n\, \mu^{2-n}\, \rho_o^{n-1}\, |\vec{v}|^n \frac{\vec{v}}{|\vec{v}|} \\ &= -\kappa\, d^n\, \mu^{2-n}\, \rho_o^{n-1}\, |\vec{v}|^{n-1}\, \vec{v}\end{aligned} \tag{B.10}$$

Gravitational force is directed vertically downward, and for a particle of density ρ in a medium of density ρ_o, it is given by

$$\vec{F}_g = -\alpha_v\, d^3\, (\rho - \rho_o)\, g\, \vec{j} \tag{B.11}$$

where $\alpha_v d^3$ is the volume of the particle. This will be written as

$$\vec{F}_g = -M' g \vec{j} \tag{B.12}$$

where M' is the effective mass of the particle. If buoyancy is negligible, then $M' = M$. Since the net force is the sum of the component forces,

$$M \ddot{\vec{r}} = \vec{D} + \vec{F}_g$$

$$= -\kappa d^n \mu^{2-n} \rho_o^{n-1} |\vec{v}|^{n-1} \vec{v} - M' g \vec{j} \tag{B.13}$$

Examination of Figure B.2 shows that

$$x = r \sin\theta \sin\phi \tag{B.14}$$

$$y = r \cos\theta \tag{B.15}$$

$$z = r \sin\theta \cos\phi \tag{B.16}$$

Thus,

$$\vec{v} = (u \sin\theta \sin\phi - V_w \sin\alpha)\vec{i} + u \cos\theta \vec{j}$$

$$+ (u \sin\theta \cos\phi - V_w \cos\alpha)\vec{k} \tag{B.17}$$

and

$$v^2 = \vec{v} \cdot \vec{v}$$

$$= u^2 - 2 u V_w \sin\theta \cos(\phi - \alpha) + V_w^2 \tag{B.18}$$

Further,

$$|\vec{v}|^{n-1} = (v^2)^{\frac{n-1}{2}}$$

$$= \left[u^2 - 2\,u\,V_w \sin\theta \cos(\phi - \alpha) + V_w^2\right]^{\frac{n-1}{2}} \qquad (B.19)$$

and finally,

$$M\,\vec{\ddot{r}} = -K\,d^n\,\mu^{2-n}\,\rho_o^{n-1}\left[u^2 - 2\,u\,V_w \sin\theta \cos(\phi - \alpha) + V_w^2\right]^{\frac{n-1}{2}}\left[(u \sin\theta \sin\phi - V_w \sin\alpha)\,\vec{i} + u \cos\theta\,\vec{j} + (u \sin\theta \cos\phi - V_w \cos\alpha)\,\vec{k}\right] - M'\,g\,\vec{j} \qquad (B.20)$$

The corresponding orthogonal components can now be separated to give three simultaneous equations. For $n = 2$,

$$M\,\ddot{x} = -K\,d^2\,\rho_o\left[u^2 - 2\,u\,V_w \sin\theta \cos(\phi - \alpha) + V_w^2\right]^{1/2}(u \sin\theta \sin\phi - V_w \sin\alpha) \qquad (B.21)$$

$$M\,\ddot{y} = -K\,d^2\,\rho_o\left[u^2 - 2\,u\,V_w \sin\theta \cos(\phi - \alpha) + V_w^2\right]^{1/2}(u \cos\theta) - M'\,g \qquad (B.22)$$

$$M \ddot{z} = -\kappa d^2 \rho_o \left[u^2 - 2 u V_w \sin\theta \cos(\phi - \alpha) + V_w^2\right]^{1/2} (u \sin\theta \cos\phi - V_w \cos\alpha) \quad (B.23)$$

For $n = 1$,

$$M \ddot{x} = -\kappa d \mu (u \sin\theta \sin\phi - V_w \sin\alpha) \quad (B.24)$$

$$M \ddot{y} = -\kappa d \mu \dot{y} - M' g \quad (B.25)$$

$$M \ddot{z} = -\kappa d \mu (u \sin\theta \cos\phi - V_w \cos\alpha) \quad (B.26)$$

For $n = 2/3$,

$$M \ddot{x} = -\kappa d^{2/3} \mu^{4/3} \rho_o^{-1/3} \left[u^2 - 2 u V_w \sin\theta \cos(\phi - \alpha) + V_w^2\right]^{-1/6} (u \sin\theta \sin\phi - V_w \sin\alpha) \quad (B.27)$$

$$M \ddot{y} = -\kappa d^{2/3} \mu^{4/3} \rho_o^{-1/3} \left[u^2 - 2 u V_w \sin\theta \cos(\phi - \alpha) + V_w^2\right]^{-1/6} (u \cos\theta) - M' g \quad (B.28)$$

$$M \ddot{z} = -\kappa d^{2/3} \mu^{4/3} \rho_o^{-1/3} \left[u^2 - 2 u V_w \sin\theta \cos(\phi - \alpha) + V_w^2\right]^{-1/6} (u \sin\theta \cos\phi - V_w \cos\alpha) \quad (B.29)$$

Making use of the relations in Equations B.14 through

B.16, Equations B.21 through B.29 become:

For $n = 2$,

$$M \ddot{x} = -\kappa d^2 \rho_o \left[\frac{\dot{x}^2}{\sin^2 \theta \sin^2 \phi} - \frac{2 \dot{x} V_w}{\sin \phi} \cos (\phi - \alpha) + V_w^2 \right]^{1/2} (\dot{x} - V_w \sin \alpha) \quad (B.30)$$

$$M \ddot{y} = -\kappa d^2 \rho_o \left[\frac{\dot{y}^2}{\cos^2 \theta} - 2 \dot{y} V_w \tan \theta \cos (\phi - \alpha) + V_w^2 \right]^{1/2} \dot{y} - M' g \quad (B.31)$$

$$M \ddot{z} = -\kappa d^2 \rho_o \left[\frac{\dot{z}^2}{\sin^2 \theta \cos^2 \phi} - \frac{2 \dot{z} V_w}{\cos \phi} \cos (\phi - \alpha) + V_w^2 \right]^{1/2} (\dot{z} - V_w \cos \alpha) \quad (B.32)$$

For $n = 1$,

$$M \ddot{x} = -\kappa d \mu (\dot{x} - V_w \sin \alpha) \quad (B.33)$$

$$M \ddot{y} = -\kappa d \mu \dot{y} - M' g \quad (B.34)$$

$$M \ddot{z} = -\kappa d \mu (\dot{z} - V_w \cos \alpha) \quad (B.35)$$

For $n = 2/3$,

$$M \ddot{x} = -\kappa d^{2/3} \mu^{4/3} \rho_o^{-1/3} \left[\frac{\dot{x}^2}{\sin^2 \theta \sin^2 \phi} - \frac{2 \dot{x} V_w}{\sin \phi} \cos (\phi - \alpha) + V_w^2 \right]^{-1/6} (\dot{x} - V_w \sin \alpha) \quad (B.36)$$

$$M\ddot{y} = -\kappa\, d^{2/3}\, \mu^{4/3}\, \rho_o^{-1/3} \left[\frac{\dot{y}^2}{\cos^2\theta} - 2\dot{y} V_w \tan\theta \cos(\phi - \alpha) + V_w^2 \right]^{-1/6} \dot{y} - M' g \qquad (B.37)$$

$$M\ddot{z} = -\kappa\, d^{2/3}\, \mu^{4/3}\, \rho_o^{-1/3} \left[\frac{\dot{z}^2}{\sin^2\theta \cos^2\phi} - \frac{2\dot{z} V_w}{\cos\phi} \cos(\phi - \alpha) + V_w^2 \right]^{-1/6} (\dot{z} - V_w \cos\alpha) \qquad (B.38)$$

If the wind velocity, $\vec{V}_w$, is zero and the motion is put in the xy-plane, these sets of equations become:

For $n = 2$,

$$M\ddot{x} = -\kappa\, d^2\, \rho_o \frac{\dot{x}^2}{\sin\theta} \qquad (B.39)$$

$$M\ddot{y} = -\kappa\, d^2\, \rho_o \frac{\dot{y}^2}{\cos\theta} - M' g \qquad (B.40)$$

For $n = 1$,

$$M\ddot{x} = -\kappa\, d\, \mu\, \dot{x} \qquad (B.41)$$

$$M\ddot{y} = -\kappa\, d\, \mu\, \dot{y} - M' g \qquad (B.42)$$

For $n = 2/3$,

$$M\ddot{x} = -\kappa\, d^{2/3}\, \mu^{4/3}\, \rho_o^{-1/3} (\sin\theta)^{1/3} \dot{x}^{2/3} \qquad (B.43)$$

$$M\ddot{y} = -\kappa\, d^{2/3}\, \mu^{4/3}\, \rho_o^{-1/3} (\cos\theta)^{1/3} \dot{y}^{2/3} - M' g \qquad (B.44)$$

$M\ddot{z}$ in all of these cases is zero.

In the case $n = 1$, the Equations B.33 through B.35 and B.41 through B.42 can be integrated; however, this is a special case, and for other values of n the equations are coupled and nonlinear. Therefore, approximate methods are required. For small, heavy particles the $n = 2$ regime is the most important. For the condition of no wind and vertical motion only, Equations B.30 through B.32 or B.39 through B.40 can be integrated in closed form. For two approximate solutions, see Section B.4.

B.3 TERMINAL VELOCITIES

The relation $M \ddot{\vec{r}} = \vec{D} + \vec{F}_g$ implies that when $\vec{D} = \vec{F}_g$ the acceleration is zero, leaving velocity constant. This equilibrium velocity is called the terminal velocity. The vector nature of the defining relation means that terminal velocity is confined to vertical motion; however, the numerical value representing the terminal velocity of a given particle in a given medium is useful in cases of nonvertical motion.

For vertical motion, the force due to gravity is

$$\vec{F}_g = -\alpha_v d^3 (\rho - \rho_o) g \bar{j} \qquad \text{(B.11)}$$

and the drag force is

$$\vec{D} = -\kappa\, d^{n}\, \mu^{2-n}\, \rho_o^{n-1}\, |\vec{v}|^{n-1}\, \vec{v} \qquad \text{(B.10)}$$

The terminal velocities for the three values of n considered in this appendix are as follows:

For $n = 2$ (turbulent),

$$v_{tu} = \kappa_t \left(\frac{\rho - \rho_o}{\rho_o}\right)^{1/2} d^{1/2} \qquad \text{(B.45)}$$

For $n = 1$ (streamline),

$$v_s = \kappa_s \left(\frac{\rho - \rho_o}{\rho_o}\right) d^2\, \mu^{-1} \qquad \text{(B.46)}$$

For $n = 2/3$ (intermediate),

$$v_i = \kappa_i\, \rho_o^{1/2}\, (\rho - \rho_o)^{3/2}\, d_o^{7/2}\, \mu^2 \qquad \text{(B.47)}$$

The κ's are dependent upon particle shape. The effective diameter d_o in B.47 is empirical and is given by

$$d_o = d - \zeta\, \bar{d} \qquad \text{(B.48)}$$

where d is the true diameter, $\bar{d}$ is given by

$$\bar{d} = \sqrt[3]{\frac{36\, \mu^2}{g\, \rho_o\, (\rho - \rho_o)}} \qquad \text{(B.49)}$$

and ζ has been empirically determined to be 0.4 for

spheres and 0.28 for irregular quartz particles, expressed in centimeter-gram-second units.

Experimental work on terminal velocities of irregular crushed quartz particles (Reference 17) has shown that particles smaller than about 25 microns obey the streamline flow conditions, while those between 85 and 2,000 microns exhibit terminal velocities which vary linearly with diameter. Larger particles show turbulent flow. For these larger particles, resistance increases proportional to the square of the diameter and weight increases proportional to the cube of the diameter; consequently, drag becomes relatively less important.

Very fine particles of diameter smaller than the mean free path of air molecules require a correction to the observed velocity to calculate drag. This correction is

$$v = \frac{1}{18} g d^3 \left(\frac{\rho - \rho_o}{\mu}\right)\left(1 + \frac{\kappa \lambda}{d}\right) \qquad (B.50)$$

where κ is a constant (0.86 for air) and λ is the mean free path of the air molecules.

B.4 APPROXIMATE SOLUTIONS TO THE EQUATIONS OF MOTION

Since the case $n = 1$ is the only one for which the

equations of motion can be integrated in closed form, approximate procedures are necessary for the more normal case in which this value of n does not apply. Typically, these involve numerical methods, assumptions to linearize or decouple the equations, or both. The results are then tabulated in parametric form, as, for example, in artillery firing tables.

For firing tables, one method used is the following: Let θ_1 be the angle between the particle's velocity vector and the horizontal. Then

$$\frac{d\theta_1}{dt} = -\frac{g}{u} \cos \theta_1 \ , \ \theta_1 < 50 \text{ degrees} \qquad \text{(B.51)}$$

This approximate relation and the assumption that the drag coefficient is a constant give

$$\dot{x} = \kappa \left(\sec^3 \theta_1\right) \dot{\theta}_1 \qquad \text{(B.52)}$$

or

$$\frac{dv_x}{dt} = \kappa \sec^3 \theta_1 \frac{d\theta_1}{dt}$$

which yields

$$v_x \Big]_{v_x}^{v_o} = \kappa \left\{ \frac{\sin \theta_1}{2 \cos^2 \theta_1} + \frac{1}{2} \log \tan \left(\frac{\pi}{4} + \frac{\theta_1}{2} \right) \right\} \Bigg]_{\theta_1}^{\theta_{1_o}} \qquad \text{(B.53)}$$

This can be solved for numerical values by the method of quadratures.

Another approximation for entirely different purposes is given in Reference 18. Suppose a vertically falling raindrop at terminal velocity falls into a layer of air with a horizontal motion perpendicular to the raindrop's path. The assumption that the raindrop's vertical motion remains unchanged gives the following results:

Let v_t = vertical velocity = constant

v_x = horizontal velocity of raindrop

$$D = \kappa v^2 \tag{B.54}$$

$$-M \frac{dv_x}{dt} = \kappa v_x (v_x^2 + v_t^2)^{1/2} \tag{B.55}$$

Integration of Equation B.55 from initial velocity v_{xi} to v_x yields

$$t = \frac{M}{\kappa v_t} \left\{ \ln \left[\frac{v_t + (v_x^2 + v_t^2)^{1/2}}{v_x} \right] - \ln \left[\frac{v_t + (v_{xi}^2 + v_t^2)^{1/2}}{v_{xi}} \right] \right\} \tag{B.56}$$

where t is the elapsed time between the two limits.

$$v_x = \frac{dx}{dt} = \frac{2\, v_t \exp\left(\frac{t\, \kappa\, v_t}{M} + A\right)}{\exp 2\left(\frac{t\, \kappa\, v_t}{M} + A\right) - 1} \qquad \text{(B.57)}$$

where

$$A = \ln\left[\frac{v_t + (v_{xi}^2 + v_t^2)^{1/2}}{v_{xi}}\right] \qquad \text{(B.58)}$$

The horizontal distance traveled in time t is found from a further integration to be

$$x = \frac{M}{\kappa}\left[\ln \tanh\left(\frac{A}{2} + \frac{t\, \kappa\, v_t}{2\, M}\right) - \ln \tanh\left(\frac{A}{2}\right)\right] \qquad \text{(B.59)}$$

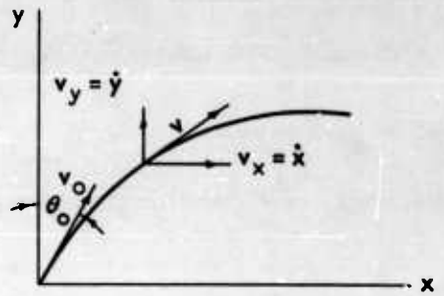

Figure B.1 Coordinate system for vacuum trajectory.

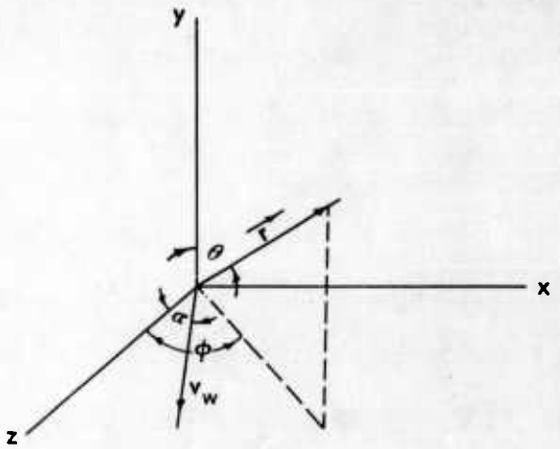

Figure B.2 Coordinate system for general trajectory analysis.

APPENDIX C*

GEOLOGIC OBSERVATIONS OF THE JOHNIE BOY CRATER LIP

C.1 GENERAL

Three trenches, one each on the north, south, and east sides of the crater (see Figure 2.8 of main text), were excavated down to or below original ground surface. These trenches, trending along radials projected from GZ, extended to the approximate limit of the crater lip.

C.2 CRITERIA FOR RECOGNITION OF ORIGINAL GROUND SURFACE

Observations of the walls of the trenches indicated that, although there was no pronounced stratification of materials, there were slight and subtle differences in lithology, color, and consistency which permitted the recognition of several "beds" or "layers" within the alluvium. These layers, present in all trenches, were numbered in consecutive order from uppermost (youngest) to lowermost (oldest) and are illustrated in Figures C.1 through C.5. The attitude and sequence of these layers were used to determine the amount of uplift and deformation caused by the explosion.

---

* Prepared by R. W. Hunt, R. T. Saucier, and W. B. Steinriede, Jr., WES Soils Division.

The general location of the postshot (uplifted original) ground surface was determined by inference from the sequence of layers of alluvium. The precise location of this surface could be obtained at various points in the trench walls by noting the locations of grass, roots, stems, and occasionally fragments of cloth or other types of litter.

C.3 TRENCH OBSERVATIONS

C.3.1 East Wall of North Trench. As shown in Figure C.1, there were two sequences of beds or layers separated by a shear plane which dipped away from the apparent crater at an angle of about 40 degrees. The postshot ground surface had been displaced upward at least 4 feet near the lip crest and had deformed in the vicinity of the shear plane.

The warping of the postshot ground surface just north of the shear plane and the configuration of the layers in the vicinity of the shear plane suggest that the northernmost sequence was uplifted and tightly folded before the shear plane developed. The shear plane appears to be the result of the innermost (southernmost) sequence being thrust outward and beneath the outermost sequence.

C.3.2 East Wall of South Trench. In the approximately

16 to 18 ft^2 of trench wall not obscured by talus, it was possible to define a situation in which the alluvial sequence had been completely overturned or folded over (Figure C.2). The three layers of alluvium which occurred below the original ground surface were present in inverted order overlying a zone in which the order was still preserved but slightly uplifted. The fold axis was preserved and is apparent both in the schematic diagram and in the accompanying photograph. The material between the two segments of original ground surface was a mixture of loose, sandy silt, gravel, and grass roots, and it probably represented a deposition of ejecta which occurred before the foldover was completed.

C.3.3 West Wall of South Trench. A small, talus-free exposure in this wall revealed that the alluvial sequence had been uplifted to an angle of about 65 to 70 degrees (see Figure C.3). The beds occurred about 4 to 5 feet higher than they did in the opposite wall of the trench, which was about 15 feet to the east, and they actually protruded about 6 inches above the ejecta surface.

Because of the obscuring ejecta and talus cover, it was not possible to determine if foldover occurred at this

point. There was no indication of a repeated inverted sequence of layers lying beyond the mapped sequence (in a direction away from GZ); the high angle to which the layers were uplifted does suggest, however, that foldover may have occurred.

C.3.4 West Wall of North Trench. A small exposure in this trench wall (Figure C.4) exhibited a normal sequence of alluvial layers overlain by an inverted sequence. The two segments of the original ground surface were in contact, with no separating layer of ejecta as shown in Figure C.2.

In this instance, the repeated sequence of beds is strong--but not conclusive--evidence that foldover occurred. Since an actual fold axis was not identified, there is a possibility that the inverted sequence represented a large block of alluvium which was ejected during the explosion and landed intact but inverted.

C.3.5 South Wall of East Trench. An arcuate exposure here revealed two steeply tilted sequences of alluvium: an innermost sequence in normal order and an outermost sequence in inverted order (Figure C.5). The two segments of original ground surface were in direct contact with one another and dipped away from the crater at approximately 70 degrees.

The lip crest of this wall was formed by a mass of layer 2 which protruded through the ejecta.

Although the absence of a fold axis again prevented the positive identification of foldover, the high angle to which the beds or layers were tilted and the length along which the back-to-back ground surfaces could be traced (about 7 feet) are strong indications that foldover occurred.

C.4 GENERAL OBSERVATIONS AROUND CRATER

The upper slopes of the apparent crater were covered with fallback. This material, consisting of loose, tan silt, sand, gravel, and cobbles, masked for the most part the uplifted beds or layers of alluvium. Around almost the entire crater, the lip crest was characterized by steep, outward-dipping exposures of layered alluvium. The general appearance was that of an irregular, roughly circular "hogback" ridge. At each of the measured sections, the only layers exposed in this ridge were layers 1 and 2. In all cases, layer 3 was covered with ejecta or talus. The rather steeply dipping uppermost 10 to 15 feet of the ejecta surface (immediately outward from the lip crest) probably directly reflected the underlying tilted alluvial sequences.

The angle of repose of the ejecta in this area was occasionally as high as 35 to 40 degrees.

C.5 CONCLUSIONS

Observations in the trenches and around the crater indicate that in all cases the originally horizontal or nearly horizontal layers of alluvium were displaced upward and outward by the force of the explosion. Although warping of beds and layers may have been most common, in at least one case (Figure C.1) a large block of alluvium was thrust beneath another along a well-defined shear plane.

In addition to the uplifting, or upthrusting, of layers, there were several examples of complete foldover, or overturning of layers. Additional excavation around the crater would probably reveal that this foldover was a rather common occurrence.

Because of the discontinuous occurrences of foldover and the shearing and distortion of the alluvium, it is not possible to accurately predict the behavior and degree of upthrust of the original ground surface which will occur as the result of a near-surface detonation such as the Johnie Boy event.

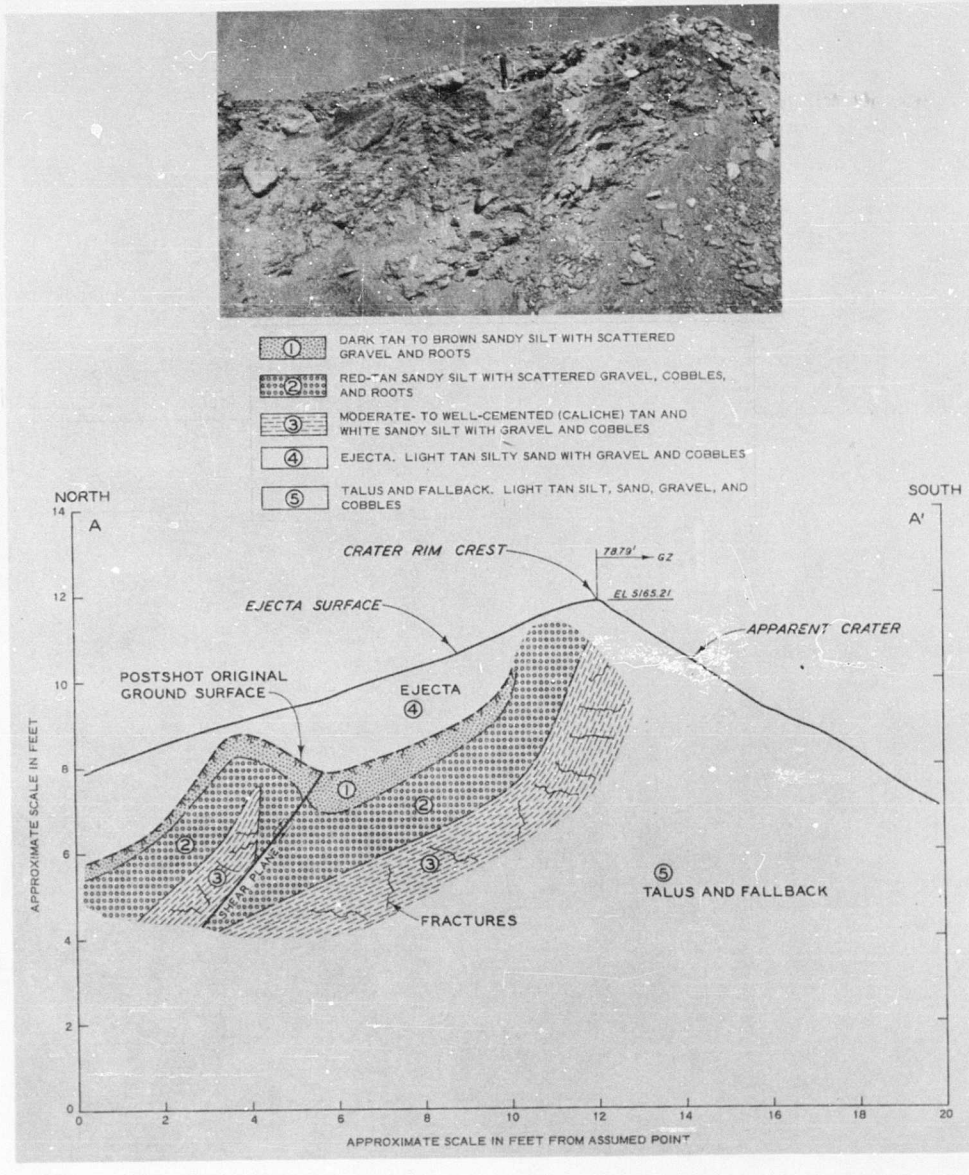

Figure C.1 Photograph and schematic diagram of exposed beds in east wall of north trench.

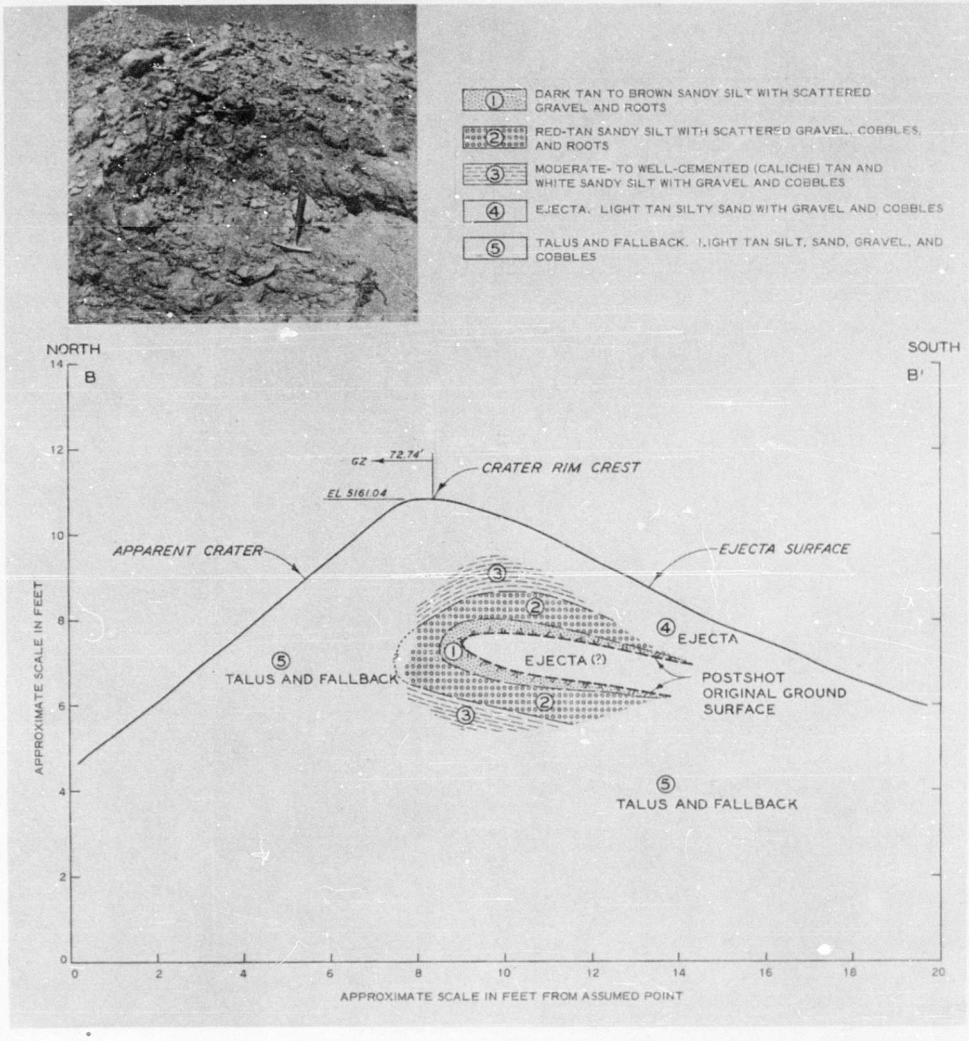

Figure C.2 Photograph and schematic diagram of exposed beds in east wall of south trench.

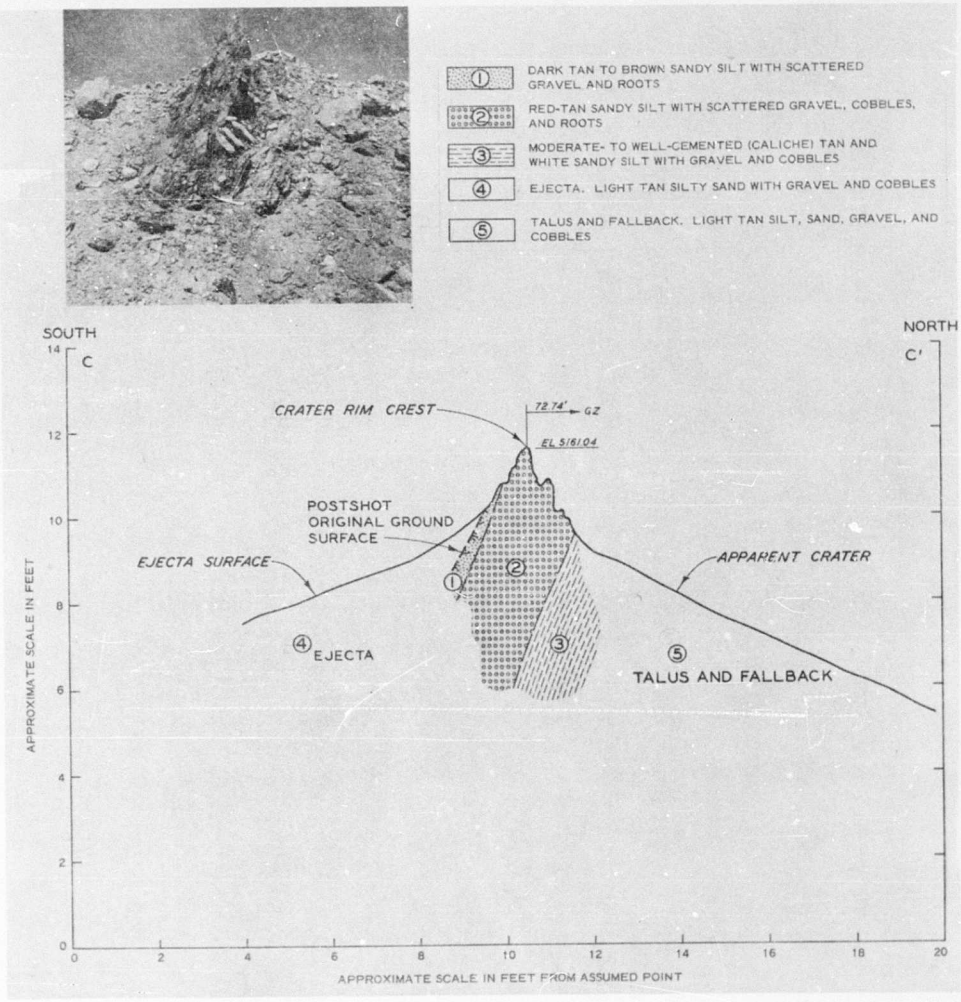

Figure C.3 Photograph and schematic diagram of exposed beds in west wall of south trench.

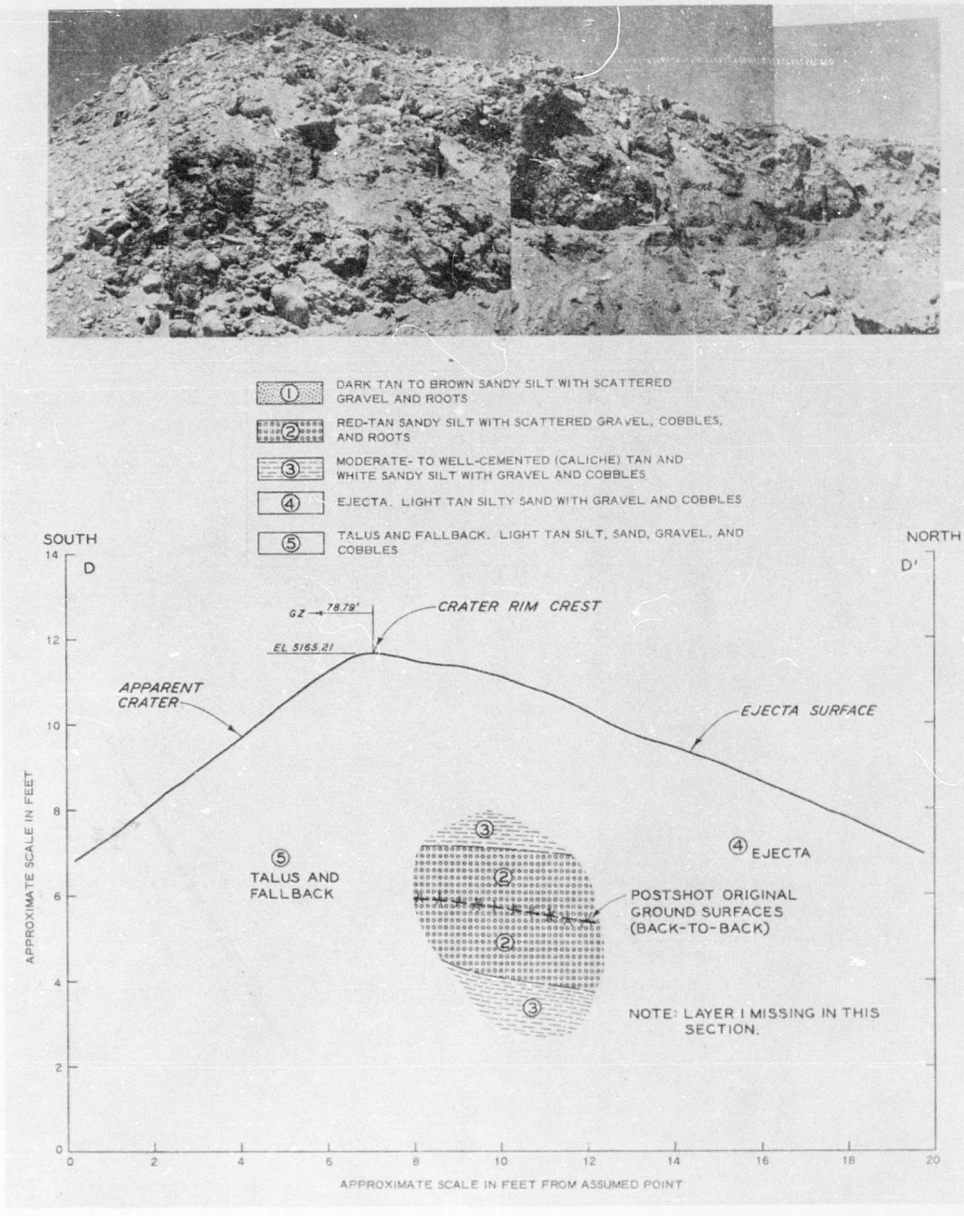

Figure C.4 Photograph and schematic diagram of exposed beds in west wall of north trench.

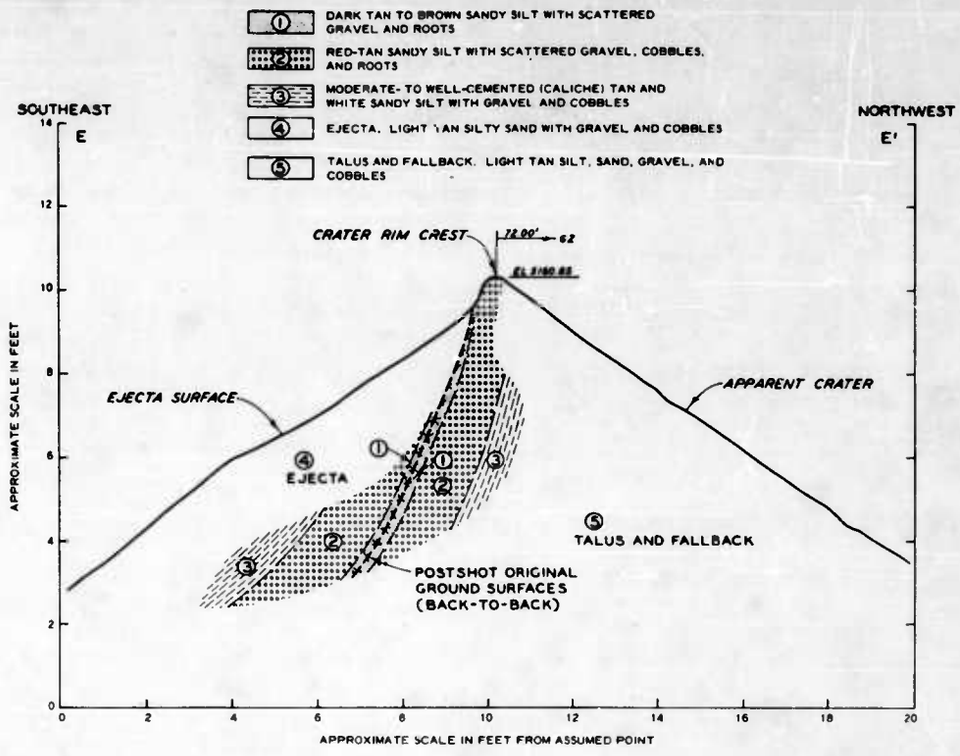

Figure C.5 Schematic diagram of exposed beds in south wall of east trench.

REFERENCES

1. Engineering Research Associates, Inc.; "Underground Explosion Test Program"; Technical Report Nos. 4 and 5, Volume I (30 August 1952 and 15 February 1953) and Final Report Volumes I and II (30 August 1952 and 30 April 1953); 1902 West Minnehaha Ave., St. Paul W4, Minn., or 507 18th St. South, Arlington, Va.; North Central Publishing Co., St. Paul, Minn.; Unclassified.

2. R. H. Carlson and W. A. Roberts; unpublished paper "Distribution of Ejecta from Cratering Explosions"; April 1963; Boeing Airplane Co., Seattle 24, Wash.; Unclassified.

3. D. J. Kempster; unofficial draft "Surface Burst of a 100 Ton TNT Hemispherical Charge (1961), Crater and Ejecta Deposit Measurements"; Suffield Technical Note No. 85; 9 April 1962; Suffield Experimental Station, Ralston, Alberta, Canada; Unclassified.

4. R. H. Carlson and W. A. Roberts; "Ejecta Study of 100-Ton Suffield Explosive Cratering Shot"; August 1962; Boeing Airplane Co., Seattle 24, Wash.; Unclassified.

5. R. H. Carlson; "Local Distribution of Material Ejected by Surface Explosions: White Tribe Interim Report"; August 1961; Boeing Airplane Co., Seattle 24, Wash.; Unclassified.

6. W. A. Roberts; "Distribution of Debris Ejected by the Stagecoach Series of High Explosive Cratering Bursts"; October 1961; Boeing Airplane Co., Seattle 24, Wash.; Unclassified.

7. R. H. Carlson and W. A. Roberts; "Ejecta Studies--Sedan Event"; December 1962; Boeing Airplane Co., Seattle 24, Wash.; Unclassified.

8. A. J. Chabai and R. H. Bishop; "Project Stagecoach: 20-Ton HE Cratering Experiments in Desert Alluvium; Final Report"; May 1962; Chapter 4 (Particulate Distribution) and Chapter (Missile Hazard from Partly Contained Explosions); Sandia Corp., Sandia Base, Albuquerque, N. Mex.; Unclassified.

9. A. J. Chabai; "Project Buckboard: 20-Ton and 1/2-Ton High Explosive Cratering Experiments in Basalt Rock; Final Report"; August 1962; Chapter 4 (Fine Particulate

Distribution); Sandia Corp., Sandia Base, Albuquerque, N. Mex.; Unclassified.

10. A. D. Rooke, Jr., and L. K. Davis; "Mass Distribution Measurements of Crater Ejecta and Dust (unpublished)"; Project 1.6, Operation Nougat, POR (WT) 1815; July 1963, USAE Waterways Experiment Station, Vicksburg, Mississippi; Unclassified.

11. H. L. Brode and R. L. Bjork; "Cratering from a Megaton Surface Burst"; RM-2600; Rand Corporation, 1700 Main St., Santa Monica, California; 30 June 1960; Unclassified.

12. F. A. Crowley; "Some Concepts for Predicting Nuclear Crater Size (U)"; Air Force Surveys in Geophysics, No. 88; Terrestrial Sciences Laboratory, Geophysics Research Directorate, Air Force Cambridge Research Center, Air Research and Development Command; February 1957; Secret-Restricted Data.

13. R. V. Whitman; "Soil Mechanics Considerations Pertinent to Predicting the Immediate and Eventual Size of

Explosion Craters"; SC-4405-(RR), Sandia Corporation; 1959; Unclassified.

14. T. B. Goode and A. L. Mathews; "Soils Survey"; **Operation Sun Beam POR-2285 Project 1.11; March 1963;** USAE Waterways Experiment Station, Vicksburg, Mississippi; Official Use Only.

15. J. M. Dallavalle; "Micromeritics"; Pitman, 1948; Unclassified.

16. G. Birkhoff; "Hydrodynamics"; Dover Publications, Inc., N. Y.; 1950; Unclassified.

17. G. Martin; "On the Diameters of Irregularly Shaped Crushed Sand Particles Lifted by Air Currents of Different Speeds and Different Temperatures"; Transactions, British Ceramics Society, Vol 23, Pages 61-109; Unclassified.

18. L. L. Weiss; "Securing More Nearly True Precipitation Measurements"; Proceedings American Society of Civil Engineers, Journal Hydraulics Division; March 1963; Unclassified.

DISTRIBUTION

Military Distribution Category 14

ARMY ACTIVITIES

1 CHIEF OF R & D DA
1 AC OF S INTELLIGENCE DA
1 CHIEF OF ENGINEERS DA
2 ARMY MATERIAL COMMAND
2 U S ARMY COMBAT DEVELOPMENTS COMMAND
1 U S ARMY CDC NUCLEAR GROUP
1 U S ARMY ARTILLERY BOARD
1 U S ARMY AIR DEFENSE BOARD
1 U S ARMY COMMAND AND GENERAL STAFF COLLEGE
1 U S ARMY AIR DEFENSE SCHOOL
1 U S ARMY CDC ARMOR AGENCY
1 U S ARMY CDC ARTILLERY AGENCY
1 U S ARMY CDC INFANTRY AGENCY
1 U S ARMY ORDNANCE & GUIDED MISSILE SCHOOL
1 U S ARMY CDC CBR AGENCY
1 ENGINEER SCHOOL
1 ARMED FORCES INSTITUTE OF PATH
1 ARMY MEDICAL RESEARCH LAB
1 WALTER REED ARMY INST OF RES
1 ENGINEER RESEARCH & DEV LAB
1 WATERWAYS EXPERIMENT STATION
1 PICATINNY ARSENAL
1 DIAMOND ORDNANCE FUZE LABORATORY
2 BALLISTIC RESEARCH LABORATORY
2 WHITE SANDS MISSILE RANGE
1 U S ARMY MOBILITY COMMAND
1 U S ARMY MUNITIONS COMMAND
1 ELECTRONICS COMMAND
1 U S ARMY ELECTRONIC PROVING GROUND
1 U S ARMY ENGINEER MISSOURI RIVER DIST
2 U S ARMY ELECTRONIC R & D LABORATORY
2 U S ARMY CDC COMBAT SERVICE SUPPORT GROUP
1 THE RESEARCH & ANALYSIS CORP
1 U S ARMY NUCLEAR DEFENSE LABORATORY
1 U S ARMY COLD REGION RES & ENG LABORATORY
1 U S ARMY CORPS OF ENG NUCLEAR CRATERING
1 UNITED STATES CONTINENTAL ARMY COMMAND
1 U S ARMY CDC COMBINED ARMS GROUP
1 DIR.OHIO RIVER DIV.LABS.US ARMY ENGR.DIV.
1 DIV.ENG.,US ARMY ENGR.DIV.MISSOURI R.
2 US ARMY ENGR.RES. & ENGR.LABS.

NAVY ACTIVITIES

2 CHIEF OF NAVAL OPERATIONS OPO3EG
1 CHIEF OF NAVAL OPERATIONS OP-75
1 CHIEF OF NAVAL OPERATIONS OP-34
3 CHIEF BUREAU OF NAVAL WEAPONS DLI-3
1 CHIEF BUREAU OF SHIPS CODE 423
1 CHIEF BUREAU OF YARDS & DOCKS CODE 74
1 DIR. US NAVAL RESEARCH LAB.
2 U S NAVAL ORDNANCE LABORATORY
1 NAVY ELECTRONICS LABORATORY
2 U S NAVAL RADIOLOGICAL DEFENSE LAB
1 U S NAVAL CIVIL ENGINEERING LABORATORY
1 U S NAVAL SCHOOLS COMMAND U S NAVAL STATION
1 U S NAVAL POSTGRADUATE SCHOOL
1 U S NAVAL SCHOOL CEC OFFICERS
1 U S NAVAL DAMAGE CONTROL TNG CENTER ABC
1 NAVAL AIR MATERIAL CENTER
1 U S NAVAL AIR DEVELOPMENT CENTER
1 U S NAVAL WEAPONS EVALUATION FACILITY
1 U S NAVAL MEDICAL RESEARCH INSTITUTE
1 DAVID W TAYLOR MODEL BASIN
1 U S NAVAL ENGINEERING EXPERIMENT STATION
1 NORFOLK NAVAL SHIPYARD
4 U S MARINE CORPS CODE A03H

AIR FORCE ACTIVITIES

2 HQ USAF AFTAC-TD
1 HQ USAF AFRDPF
1 HQ USAF AFXPDG
1 HQ USAF AFOCEKA
1 HQ USAF AFGOA
5 HQ USAF AFNINDE
1 AC OF S INTELLIGENCE HQ USAFE
1 BALLISTIC SYSTEMS DIVISION
1 HQ USAF AFMSPAA
1 TACTICAL AIR COMMAND
1 AIR DEFENSE COMMAND
1 AIR FORCE SYSTEMS COMMAND
1 RADC-RAALD,GRIFFISS AFB
1 PACIFIC AIR FORCES
1 SECOND AIR FORCE
2 AF CAMBRIDGE RESEARCH CENTER
5 AFWL WLL-3 KIRTLAND AFB
2 AIR UNIVERSITY LIBRARY
1 SCHOOL OF AVIATION MEDICINE
3 AERONAUTICAL SYSTEMS DIVISION
2 USAF PROJECT RAND
1 AIR TECHNICAL INTELLIGENCE CENTER
1 HQ USAF AFORQ
1 HQ USAF AFXPDK

OTHER DEPARTMENT OF DEFENSE ACTIVITIES

1 DIRECTOR OF DEFENSE RESEARCH AND ENGINEERING
1 ASST TO THE SECRETARY OF DEFENSE ATOMIC ENERGY
1 ADVANCE RESEARCH PROJECT AGENCY
1 WEAPONS SYSTEM EVALUATION GROUP
1 ASST SECRETARY OF DEFENSE INSTALLATION & LOGISTICS
4 DEFENSE ATOMIC SUPPORT AGENCY
1 FIELD COMMAND DASA
1 FIELD COMMAND DASA FCTG
2 WEAPONS TEST DIV.,DASA,SANDIA,WTWT-TI
1 ARMED SERVICES EXPLOSIVES SAFETY BOARD
1 JOINT TASK FORCE-8
1 COMMANDER-IN-CHIEF PACIFIC
1 COMMANDER-IN-CHIEF ATLANTIC FLEET
1 STRATEGIC AIR COMMAND
1 CINCONAD
3 ASST SECRETARY OF DEFENSE CIVIL DEFENSE
1 DIR.DEFENSE INTELLIGENCE AGENCY
20 DEFENSE DOCUMENTATION CENTER

FOR CIVILIAN DISTR CAT. A 2

1 AEROSPACE CORPORATION
1 UNITED ELECTRODYNAMICS INC PASADENA
1 SPACE TECH LAB LOS ANGELES ATTN SUSSHOLZ
1 MIT CAMBRIDGE MASS ATTN HANSON,WHITMAN
1 US COAST &GEODETIC SURVEY WASHINGTON ATTN MURPHY
1 STANFORD RESEARCH INSTITUTE ATTN VAILE
1 US GEO SURVEY DENVER COL ATTN ROACH
1 US GEO SURVEY DENVER COL ATTN PAKISER
1 HOLMES AND NARVER FOUNDATION LOS ANGELES
1 IIT RESEARCH INSTITUTE ATTN TECH. LIBRARY
1 GEN AMERICAN TRANS CORP NILES ILL
1 UNIVERSITY OF ILLINOIS ATTN NEWMARK
1 UNITED RES.SERVICES BURLINGAME,CALIF.
1 BARRY CONTROLS ATTN CAVANAUGH
1 GENERAL ELCTRIC CO DEF.ELEC.DIV.

ATOMIC ENERGY COMMISSION ACTIVITIES

3 AEC WASHINGTON TECH LIBRARY
2 LOS ALAMOS SCIENTIFIC LAB
5 SANDIA CORPORATION
10 LAWRENCE RADIATION LAB LIVERMORE
1 NEVADA OPERATIONS OFFICE,LAS VEGAS
1 DTIE OAK RIDGE,MASTER
30 DTIE OAK RIDGE SURPLUS